

Onset of runaway fragmentation of salt marshes

Orencio Duran Vincent^{1,2,4,*}, Ellen R. Herbert^{1,3}, Daniel J. Coleman¹, Joshua D. Himmelstein¹, and Matthew L. Kirwan¹

¹Virginia Institute of Marine Sciences, College of William and Mary, Gloucester Point, Virginia 23062, USA

²Texas A&M University, Department of Ocean Engineering, College Station, Texas 77843, USA

³Ducks Unlimited, Memphis, Tennessee 38129, USA

⁴Lead Contact

*Correspondence: oduranvinent@tamu.edu

Post-print of a manuscript published in One Earth
<https://doi.org/10.1016/j.oneear.2021.02.013>

SUMMARY

Salt marshes are valuable but vulnerable coastal ecosystems that adapt to relative sea level rise (RSLR) by accumulating organic matter and inorganic sediment. The natural limit of these processes defines a threshold rate of RSLR beyond which marshes drown, resulting in ponding and conversion to open waters. We develop a simplified formulation for sediment transport across marshes to show that pond formation leads to runaway marsh fragmentation, a process characterized by a self-similar hierarchy of pond sizes with power-law distributions. We find the threshold for marsh fragmentation scales primarily with tidal range and that sediment supply is only relevant where tides are sufficient to transport sediment to the marsh interior. Thus the RSLR threshold is controlled by organic accretion in microtidal marshes regardless of the suspended sediment concentration at marsh edge. This explains the observed fragmentation of microtidal marshes and suggests a tipping point for widespread marsh loss.

Keywords: wetland, sea level rise, marsh drowning, accretion, pond, sediment transport, pattern formation

1 Introduction

2 There is a growing consensus that marsh vulnerability to relative sea level rise (RSLR) is tied to inorganic sediment availability^{1–4}, where deposition of inorganic sediment increases with flooding duration, and potentially offsets sea level rise. Indeed, inorganic deposition rates have accelerated over the last century concomitant with sea level rise^{5,6} and historic marsh loss has been observed (and projected^{7,8}) mostly in sediment-poor systems^{9,10} and microtidal marshes¹¹. Modeled threshold rates of RSLR for marsh drowning, using simplified point (0-D) models, increase by 2 orders of magnitude as a function of suspended sediment concentration and tidal range^{12,13}. However, a contrasting body of work emphasizes the importance of organic matter accumulation in building marsh soils in the face of sea level rise, especially in the sediment deficient estuaries most vulnerable to sea level rise^{1,11,14–17}. Total marsh accretion rates are more strongly correlated with the organic fraction of marsh soil than the inorganic fraction¹⁴; organic matter contributes 4 times more soil volume than an equivalent mass of inorganic sediment¹⁶; and organic matter is the dominant contribution to marsh accretion by volume in many Atlantic and Gulf Coast marshes^{14–16}.

23 Competing ideas about the relative importance of organic and inorganic accretion likely reflect strong spatial gradients within marshes^{18–20}. Inorganic accretion increases with suspended sediment concentration and flooding depth, and decreases with distance to tidal channels, as reported both in the field^{21–25} and in models^{18–20,25–29}. Organic accretion is influenced by the production and decomposition of plant biomass, both of which vary spatially across marshes in response to flooding depth as well as other factors. Moreover, vegetation itself enhances inorganic sediment deposition so that organic and inorganic contributions are thoroughly inter-

twined^{30,31}. These spatial gradients of organic and inorganic deposition lead to complex patterns of marsh accretion and submergence that are sometimes difficult to explain. For example, marshes along the Blackwater River (MD, USA) are rapidly submerging despite having a higher suspended sediment concentrations measured in channels, than in nearby stable marshland^{32,33}. Elsewhere, marshes are submerging despite measured accretion rates that are similar to or exceed RSLR^{2,33}, which suggests measurements take place mostly along marsh edges, where maximum accretion rates are generally observed^{21,23,34,35}.

The complexity of organic and inorganic accretion in a marsh platform leads to the simple question: where in a marsh should organic and inorganic contributions to marsh accretion be characterized to best evaluate marsh vulnerability to RSLR? Measurements from high elevation portions of a marsh potentially underestimate future marsh accretion because inorganic accretion rates may accelerate with increased flooding duration². However, if low elevation marshes are also closest to channels, then accretion rates from low elevation portions of the marsh would overestimate accretion to the marsh as a whole, and lead to an underestimation of marsh vulnerability to RSLR.

Another issue with the interpretation of measured accretion rates is that they tend to converge towards the local rate of RSLR, as the marsh platform approaches an equilibrium elevation³⁶, which complicates the estimation of maximum accretion rates unless marshes are already drowning^{2,37}. Thus, there is a need for better numerical models that resolve the spatial complexity of marsh sediment dynamics^{4,13,19,27,28,38–40}.

A few existing process-based models (e.g.^{19,28}) capture the observed drowning of interior marshes and their conversion to ponds^{41–43}. They suggest marsh drowning, and subsequent

pond formation, is not described by a single threshold but is instead a gradual process where different portions of the marsh platform drown at different rates of RSLR. Therefore, existing models with RSLR rates just slightly faster than the threshold for drowning would produce an equilibrium state characterized by relatively few, isolated ponds, far from the channel edge.

Here, we uniquely show that there is no equilibrium state for a marsh platform once a local threshold for marsh drowning has been crossed, resulting in runaway marsh fragmentation. Theoretical considerations and field observations indicate that the threshold for marsh drowning does not change much with sediment supply in microtidal marshes, suggesting a disproportionate role of organic accretion.

Model approach

We use a one-dimensional formulation for the mass conservation of water and inorganic sediments in the absence of erosion^{4, 27, 28, 38, 39, 44}, to derive a minimal sediment transport model that captures the central physics of the system (the complete model is described in the Experimental Procedures; see Figs. S1 and S2 for examples of the solutions). This simplified model allows us to define and calculate the drowning threshold and characterize the dynamics of the ensuing marsh fragmentation without the need of spatially-explicit hydrodynamic models^{26, 27, 29, 39, 45}.

The current understanding of the onset of marsh loss is that it takes place whenever marsh depth relative to mean high water is higher than a critical value D_c above which marshes are replaced by tidal flats or ponds as the more stable morphology^{43, 46–49}. Indeed, field data suggests marsh conversion to tidal flats starts at a critical depth D_c around 35% of the tidal range δz , which corresponds to an average rescaled inundation time, i.e. fraction of time the marsh is submerged $\tau_c \approx \pi^{-1} \arccos(1 - 2D_c/\delta z)$, of about 0.4 (Fig. 1B, see Table S1 for details)^{42, 43, 46–48}.

Assuming the existence of a critical depth for marsh recovery, a general condition for the onset of local marsh drowning is when the rate R of RSLR exceeds the sum of the organic (A_o^c) and inorganic (A_i^c) accretion rates evaluated at the critical depth D_c (Fig. 1A). Because of the spatial variation of inorganic deposition, the lowest inorganic accretion rate at the critical depth thus defines the lowest threshold (R_c) for local marsh drowning: $R_c = A_o^c + \min\{A_i^c\}$.

We derive a general expression for R_c from a simplified model of the inorganic accretion rate $A_i(x, D)$ across a marsh platform with variable depth $D(x)$, as function of the distance x to the sediment sources. In the absence of erosion, we assume $A_i(x, D)$ can be written in terms of the depth-dependent rescaled average inundation time $\tau(D)$ and the depth-independent sediment concentration $\bar{C}(x)$, as $A_i(x, D) = \rho_i^{-1} w_f \tau(D) \bar{C}(x)$, where ρ_i is an average density of deposited sediments¹, w_f is an effective settling velocity and \bar{C} is defined as the local depth-averaged suspended sediment concentration (SSC) averaged over times of positive water depths in a tidal cycle (see Experimental Procedures).

In what follows we present and validate an explicit expression for the inorganic accretion rate across the marsh platform and use it to obtain the critical inorganic accretion rate for marsh drowning. We then introduce the drowning threshold,

characterize the runaway marsh fragmentation regime and discuss the effect of external parameters on marsh drowning.

Results

Exponential decay of sediment concentration

As inorganic sediments in the water column settle on the marsh surface, where erosion is assumed to be negligible²⁷, the averaged sediment concentration \bar{C} decays with the distance x from the channel or tidal flat (Fig. 2). Sediment concentration thus reaches its lowest value at the location furthest away—a distance L —from marsh edges (Fig. 2A), defined in the model as the watershed divide. This decay in sediment concentration is well approximated by an exponential function, $\bar{C}(x) = \bar{C}(0)e^{-x/L_c}$ (as proposed by²⁵ and observed by²³), with decay length L_c (see Experimental Procedures). Therefore, the inorganic accretion rate for a non-flat marsh platform can be approximated as

$$A_i(x, D(x)) \approx \rho_i^{-1} w_f \tau(D(x)) \bar{C}(0) e^{-x/L_c}, \quad (1)$$

where the average sediment concentration $\bar{C}(0)$ at the channel bank or marsh edge is proportional to the average concentration C_0 at the channel or mud flat during flood (see Fig. S3 for the proportionality factor).

The decay length L_c of the average suspended sediment concentration scales as the ratio of the tidal discharge per unit width and the effective sediment settling velocity w_f , in agreement with the scaling of the deposition length in unidirectional turbulent suspensions⁵⁰ (Experimental Procedures). We find tidal discharge per unit width scales as $L\delta z/T$, where δz is the tidal range, T is the tidal period and L is the characteristic length of the local drainage basin. Thus, the decay length has the form

$$L_c = \beta L \delta z / (T w_f), \quad (2)$$

with fitting parameter $\beta \approx 1.5$, in agreement with both numerical simulations and analytical approximations (Experimental Procedures and Fig. 2B).

We find the exponential approximation accurately describes the sediment concentration profile except in the region around the watershed divide, where tidal flow stops and the simulated average sediment concentration, and thus accretion rates, converge to zero (Fig. 2). In reality, complex tidal flows may lead to residual accretion rates in the marsh interior (e.g.²²), in which case the exponential approximation provides an upper limit to evaluate the resiliency of drowning marshes. In what follows we use the watershed divide as a formal definition of the marsh interior.

The exponential decay correctly predicts the spatial gradient in the average sediment concentration and inorganic accretion rates for a wide variety of salt marshes (Fig. 3), including low-elevation micro-tidal marshes in the Virginia eastern shore (Phillips Creek)³⁴ and Georgia³⁵, and meso- and macro-tidal marshes in Plum Island, MA⁵¹, Norfolk, UK²¹ and in the Bay of Fundy, CA⁵² (see Experimental Procedures for further details on the analysis and interpretation of inorganic accretion data).

The scaling of L_c with the tidal range δz (Eq. 2) means that suspended sediments deposit closer to channels (or tidal flats) at lower tidal ranges, whereas they are more homogeneously distributed at higher tidal ranges. This is consistent with the

180 trend observed in field measurements (Fig. 3), in particular the
 181 contrast between the almost homogeneous inorganic accretion
 182 in the Bay of Fundy, CA⁵² ($\delta z = 11\text{m}$), and the noticeable decay
 183 observed in Phillips Creek, US²⁵ ($\delta z = 2\text{m}$).

184 Critical inorganic accretion rate

185 The scaling of the sediment decay length L_c with the local
 186 drainage basin length L (Eq. 2) follows from the approximate
 187 scale invariance of tidal flows⁴⁴, i.e. faster flows—and increas-
 188 ing sediment advection—on larger basins. This scale invari-
 189 ance, where sediments are deposited farther away from the
 190 channels in large basins as compared to small ones (Fig. S4),
 191 has one important implication: the lowest inorganic accre-
 192 tion rate at the critical depth D_c for marsh conversion to tidal
 193 flats $A_i^c(L) \equiv A_i(L, D_c)$, reached at the watershed divide $x = L$
 194 (Eq. 1), does not depend on drainage basin size L and can be
 195 evaluated without the need of spatially-explicit hydrodynamic
 196 models. Indeed, after substituting the scaling for the decay
 197 length we get for the critical inorganic accretion rate:

$$A_i^c(L) = A_i^c(0)e^{-1/\ell_c}, \quad (3)$$

198 where $\ell_c = L_c/L = \beta/w_f^+$ is the rescaled decay length, which
 199 only depends on the rescaled effective falling velocity $w_f^+ =$
 200 $w_f T/\delta z$, and $A_i^c(0) \equiv A_i(0, D_c)$ is the inorganic accretion rate at
 201 the critical depth in the marsh edge (Eq. 1). Using the scaling
 202 $\bar{C}(0) = r(w_f^+)C_0$ we find for the flood-ebb average sediment con-
 203 centration at the marsh edge (see Experimental Procedures),
 204 we get the explicit expression

$$A_i^c(0) = \rho_i^{-1}C_0w_f r(w_f^+)\tau_c, \quad (4)$$

205 with $\tau_c \equiv \tau(D_c)$. Thus, the critical inorganic accretion rate
 206 (Eq. 3) is completely determined by external, measurable pa-
 207 rameters, characterizing sediment supply to the marsh (C_0),
 208 effective sediment properties (w_f and ρ_i) and tides (δz and T).

209 An important consequence of the physical mechanisms
 210 driving sediment redistribution across the marsh platform, as
 211 summarized in Eq. 3, is that the critical inorganic accretion
 212 rate strongly depends on the tidal range (Fig. 4). For typical
 213 values of the parameters, $A_i^c(L)$ becomes negligible for tidal
 214 ranges $\delta z < 1\text{m}$ regardless of the sediment supply (Fig. 4),
 215 in stark contrast to the critical inorganic accretion rate at the
 216 marsh edge $A_i^c(0)$ (Fig. 4A). More generally, for most microtidal
 217 marshes ($\delta z < 1.5\text{m}$) the predicted critical accretion rate in the
 218 marsh interior ($A_i^c(L)$) is below common rates of RSLR (2.5-
 219 5mm/yr) (Fig. 4B) and organic accretion becomes crucial for
 220 marsh survival.

221 Threshold for marsh drowning and the onset of runaway 222 marsh fragmentation

223 The marsh accretion rate at the critical depth in the marsh
 224 interior, $A_o^c + A_i^c(L)$, defines the lowest threshold for marsh
 225 drowning R_c (Fig. 5A). When relative sea level rises at a lower
 226 rate ($R < R_c$), marshes are stable by definition and bare areas
 227 with an elevation above the critical depth can recover with
 228 time⁴². When relative sea level rises at a faster rate ($R > R_c$),
 229 interior marshes drown and form permanent ponds.

230 Simulations of the time evolution of marsh elevation $Z(x, t)$
 231 (see Experimental Procedures for model details), show marsh

232 fragmentation regime strongly depends on whether perman-
 233 ent ponds are isolated or connected to the channel network
 234 (Fig. 5A). In the first case, tidal basins and watershed divides
 235 remain unchanged and the system evolves towards a new
 236 equilibrium state (Fig. 5A, left). The portion of the marsh
 237 closer to the edge adapts to RSLR and reaches a non-uniform
 238 equilibrium marsh elevation in response to spatial gradients of
 239 sediment concentration, e.g. as in the formation of natural lev-
 240 ees⁵³. We find the equilibrium pond size scales with the size of
 241 the local basin and increases with the rate R of RSLR (Fig. 5A
 242 left, see Experimental Procedures for pond size calculation).

243 However, isolated ponds tend to connect to the channel net-
 244 work via the formation of new small channels^{41,42,49}, thereby
 245 increasing channel density and shrinking tidal basins. Based
 246 on this, we assume in our model that once ponds are deep
 247 enough they connect to channels and become a source of
 248 sediment and tidal flow (see Experimental Procedures). Re-
 249 gardless of the specific conditions for when and how ponds
 250 connect, simulations show there is no marsh equilibrium as
 251 long as permanent ponds are able to connect to the channel
 252 network. Instead, marshes experience a continuous (runaway)
 253 fragmentation at a rate controlled by the ratio R/R_c (Fig. 5A,
 254 right).

255 The runaway fragmentation can be understood as follow:
 256 although there are more channels (and connected ponds)
 257 to potentially redistribute sediments into the marsh platform,
 258 the sediment will be deposited closer to the banks as water
 259 flow slows down in the now smaller basins (see Eq. 2). As
 260 a result, the drowning threshold $R_c = A_o^c + A_i^c(L)$ is crossed
 261 around the watershed divide of the new system, leading to
 262 marsh drowning at ever smaller scales. Therefore, with time,
 263 marsh fragmentation propagates from large to small scales
 264 following the adjustment of the channel network and tidal flows,
 265 until most of the marsh is lost.

266 We can obtain an upper-bound for the threshold rate of
 267 RSLR for the onset of runaway marsh fragmentation ($R_c =$
 268 $A_o^c + A_i^c(L)$, Fig. 6) using a theoretical estimation of the max-
 269 imum contribution of organic accretion for salt marshes¹
 270 ($A_o^c \approx 3\text{mm/yr}$). This value is consistent with accretion rate
 271 data of Mid-Atlantic US salt marshes and falls within a broader
 272 range of direct and indirect estimations of organic accretion
 273 rates of marshes elsewhere (see Fig. S5 and Supplemental
 274 Experimental Procedures). Similarly to the trend of inorganic
 275 accretion rates with tidal range (Fig. 4), the predicted threshold
 276 R_c (Fig. 6) shows a fundamental vulnerability for microtidal
 277 marshes ($\delta z < 1.5\text{m}$) and marshes with relatively low sediment
 278 supply (average SSC at the channel bank or marsh edge in
 279 the range $C_0 < 20\text{g/m}^3$).

280 Self-similarity of marsh fragmentation and power-law dis- 281 tribution of pond size

282 Because pond size scales with basin size (see Experimental
 283 Procedures), the progressive shrinking of tidal basins during
 284 marsh fragmentation should lead to a self-similar hierarchy of
 285 pond sizes with a Pareto (power-law) distribution⁵⁴. Indeed, we
 286 find a power-law distribution of pond areas and a self-similar
 287 pattern of marsh loss, in both, our model simulations of marsh
 288 fragmentation (shown in Fig. 5A, where pond area is defined
 289 as the square of its length) and in rapidly submerging marshes
 290 in Blackwater, MD and Louisiana (Fig. 5), where drowning

begins near the watershed divide and propagates towards the channels⁴¹.

Interestingly, the exponent of the power-law distribution of the area of simulated ponds changes little with the rate of RSLR above the threshold R_c , and is very similar to the one obtained for small to medium-size ponds ($\lesssim 10^5 \text{m}^2$) in Blackwater⁵⁵ (Fig. 5B). The exponent (~ 1.5) is consistent with a simple 'period-doubling' mechanism, where whenever a pond connects to the channel network it creates two new ponds with half the diameter (one quarter of the area) of the 'parent' one.

The size distribution of large ponds in Louisiana⁵⁶ has a larger exponent (~ 2.5) similar to the one for similar-size ponds in Blackwater (Fig. 5B), which suggests a further scale-invariant mechanism affecting pond growth.

Discussion

Vulnerability of microtidal marshes

Although marsh vulnerability has been traditionally tied to inorganic sediment availability, we find consistently low inorganic accretion in the interior of most microtidal marshes ($\lesssim 2.5 \text{mm/yr}$, one sixth of existing predictions, e.g. ^{18,19,28}, see Fig. 4B) regardless of sediment supply. This vulnerability is highest for marshes with tidal ranges $< 1 \text{m}$ (Fig. 4B), where inorganic accretion in the marsh interior is negligible and the threshold RSLR rate seems to be completely determined by organic accretion. This explains the apparent contradiction of Blackwater marshes, where a relatively high suspended sediment concentration in the channels does not prevent drowning^{32,33}. With a tidal range $< 0.5 \text{m}$, inorganic accretion is irrelevant for the vast majority of the marsh platform. Thus, it is enough for the local rate of RSLR to be higher than the organic accretion rate to induce widespread drowning (Fig. 6). This indeed seems to be the case in both Blackwater⁵⁷, and in the Mississippi Delta, where the threshold for continuous marsh loss was estimated to be about 3mm/yr ⁵⁸, very similar to model prediction for $\delta z < 1 \text{m}$ (Fig. 6). The predicted low inorganic deposition in the marsh interior also agrees with the predominantly organic composition of sediments found in many marshes with tidal range $< 1 \text{m}$ (e.g. Blackwater, MD⁵⁷; Gulf of Mexico¹⁴).

While organic accretion is a complex function of several factors, such as plant species, water salinity, flooding frequency, water and soil temperature and composition^{10,16}, a meta-analysis of field data reveals organic accretion rates are in the range of $3.0 \pm 2.0 \text{mm/yr}$ (Fig.S5 and Supplemental Experimental Procedures), which happens to be in the range of observed RSLR rates. Therefore, it seems we currently are at the tipping point for widespread drowning of global microtidal salt marshes regardless of the local inorganic sediment supply (Fig. 6). Indeed, the model correctly predicts the drowning of Blackwater marshes and marshes in the Mississippi Delta⁵⁸, and also suggests marshes in Venice, the Virginia Eastern Shore (e.g. Phillips Creek) and Plum Island, MA, are particularly vulnerable (Fig. 6).

We thus provide a mechanistic explanation for the widely observed fragility of microtidal marshes¹¹ and show this vulnerability is intrinsic and tied to the dominant role of organic accretion. Therefore, factors altering biomass productivity and decomposition, such as eutrophication, elevated CO_2 and cli-

mate warming^{10,11,19,59}, could decide the mid-term response of global microtidal marshes, while measures aimed at increasing sediment delivery could have limited success.

Runaway marsh fragmentation

The runaway marsh fragmentation induced by the approximate scale invariance of sediment deposition⁴⁴, constitutes a new form of marsh destabilization that transforms the local crossing of the marsh drowning threshold into the onset of eventual widespread marsh loss. This mechanism only requires that connected ponds decrease the size of local drainage basins, regardless of whether they deliver sediment to the marsh platform or not. In the best case scenario depicted in Fig. 5A, connected ponds redistribute inorganic sediment as effective as large channels or mud flats, which is not the case in reality. Any decrease in sediment delivered by connected ponds leads to lower inorganic accretion rates on the surrounding marshes, thereby accelerating marsh drowning.

The scale invariance of sediment deposition, where sediment is deposited closer to the banks in smaller basins, underpinning the runaway marsh fragmentation is consistent with observations that an increased density of artificial channels does not increase overall sedimentation (e.g. Louisiana⁶⁰) and in some cases resulted in subsidence (e.g. New England⁶¹). Furthermore, the predicted acceleration of marsh fragmentation with the rate of RSLR (Fig. 5A) is consistent with the rapidly increased rate of historic marsh loss measured in the Mississippi Delta as RSLR accelerated⁵⁸.

The marsh fragmentation mechanism explains the formation of a broad range of pond sizes, and predicts that their size distribution should follow a power-law, in agreement with data from Blackwater marshes (Fig 5B). It also predicts a particular temporal sequence of marsh fragmentation, as large initial ponds eventually lead to smaller ones at a rate increasing with the rate of RSLR relative to the drowning threshold (Fig. 5A), and suggests the area of the larger ponds depends on the initial distribution of tidal basin areas. This multi-scale mechanism complements existing models of pond growth driven by lateral expansion instead of RSLR^{40,62}.

Conclusions

We derive a simplified model of sediment transport in the absence of erosion that explains patterns of sediment deposition and marsh vulnerability in a wide variety of conditions. Our model leads to an analytical prediction of inorganic accretion that complements direct measurements of accretion, which necessarily reflect historical rather than future environmental conditions². We predict a new form of marsh destabilization characterized by a progressive fragmentation of the marsh platform, triggered by the drowning of interior marshes. The threshold for this runaway marsh fragmentation is much lower than existing predictions^{13,63} and is largely decoupled from inorganic sediment supply in microtidal environments, which explains the observed fragility of microtidal marshes. Beyond microtidal marshes, the much-lower marsh fragmentation thresholds predicted by our model suggest a re-evaluation of the resiliency of global marshes under current and future scenarios⁶³.

405 Experimental Procedures

406 Resource Availability

407 Lead Contact

408 Further information and requests for resources and reagents
409 should be directed to and will be fulfilled by the Lead Contact,
410 Orencio Duran Vinent (oduranvinent@tamu.edu)

411 Materials Availability

412 The original (unpublished) data used in this study is available
413 in Table S2.

414 Data and Code Availability

415 This study did not generate new datasets. The MatLab code
416 integrating the model equations is available upon request from
417 the Lead Contact.

418 Minimal model of sediment transport on a marsh

419 We consider one-dimensional depth-integrated mass conser-
420 vation equations for tidal water discharge per unit width $Q(x, t)$
421 and depth-averaged suspended sediment concentration of
422 inorganic sediments $C(x, t)$ over a marsh surface with eleva-
423 tion $Z(x)$ relative to mean sea level (MSL). Assuming, (i) a
424 quasi-static tidal propagation with average water elevation
425 (relative to MSL) $\eta(t) = (\delta z/2) \cos(2\pi t/T)$ with tidal range δz
426 and period T , (ii) no net sediment erosion, and (iii) negligible
427 lateral diffusion, the conservation of suspended sediments
428 reads^{4, 27, 28, 38, 39, 44}:

$$\partial_t(HC) + \partial_x(QC) = -w_f C \quad (5)$$

429 where x is the distance from the marsh edge (channel bank or
430 tidal flat) along the flow direction, $H(x, t) = \eta(t) - Z(x)$ is local
431 water depth and w_f is an effective sediment falling velocity. Q is
432 obtained from the continuity equation $\partial_x Q = -\partial_t \eta$ assuming no
433 water flux ($Q(L, t) = 0$) at the watershed divide $x = L$: $Q(x, t) =$
434 $\partial_t \eta (L - x) = -\delta z L T^{-1} \pi \sin(2\pi t/T) (1 - x/L)$. Q thus scales as
435 $\delta z L/T$.

436 For simplicity, Eq. 5 is numerically integrated for a flat
437 marsh surface during positive water depths ($H(t) > 0$) using
438 two boundary conditions, a constant suspended sediment
439 concentration ($C(0, t) = C_0$) at the channel bank ($x = 0$) dur-
440 ing flood ($t < 0$) and no sediment crossing the watershed
441 divide ($C(L, t) = 0$) during ebb ($t > 0$). Using rescaled time
442 ($t^+ = t/T$) and distance ($x^+ = x/L$), the rescaled concentra-
443 tion $C(x^+, t^+)/C_0$ for a given marsh elevation Z is only function
444 of one dimensionless number: the rescaled effective falling
445 velocity $w_f^+ = w_f T/\delta z$ (Fig. S1).

446 Approximation for the tidal-averaged sediment transport

447 A further simplification is obtained by averaging Eq. 5, valid for
448 a non-flat marsh elevation $Z(x)$, over times of positive water
449 depths in a tidal cycle, and neglecting the changes to the
450 gradient of sediment fluxes (QC) due to variable elevation,

$$\partial_x \overline{QC} \approx -w_f \overline{C}, \quad (6)$$

451 where the bar denotes an average of the form

$$\overline{C}(x) \equiv \tau(D)^{-1} \int_{-\tau(D)/2}^{\tau(D)/2} C(x, t^+) dt^+ \quad (7)$$

where $\tau(D)$ is the rescaled local inundation time and $D(x) =$ 452
 $\delta z/2 - Z(x)$ is the local depth. 453

454 Because the main effect of a non-flat marsh platform is to
455 change the local inundation time $\tau(D)$, this averaging removes,
456 in a first approximation, the dependence on marsh elevation
457 and thus its solution has the form $\overline{C} \approx \overline{C}(x)$. Therefore, we can
458 use the numerical solution of Eq. 5 for a flat marsh to obtain a
459 correlation between the average sediment flux per unit width
460 (\overline{QC}) and the average suspended sediment concentration (\overline{C}).
461 This correlation is expected when transport is dominated by
462 advection instead of diffusion.

463 Indeed, in the range $x/L \lesssim 0.6$, we find (see Fig. S2)

$$\overline{QC}(x) \approx \beta \delta z L T^{-1} (\overline{C}(x) - \overline{C}(L)), \quad (8)$$

464 where $\beta = 1.5$ is a fitting constant and $\overline{C}(L)$ is defined as 465
an effective sediment concentration at the watershed divide 466
 $x = L$. This definition follows from the boundary condition of no 467
average sediment transport across the watershed divide, i.e. 468
 $\overline{QC}(L) = 0$. Using Eq. 8, the total mass of sediment deposited 469
on the 1-D marsh during one tidal cycle, $\tau(D) T \int_0^L w_f \overline{C}(x) dx$,
470 can be approximated by integrating Eq. 6 as $\overline{QC}(0) \tau(D) T \approx$
471 $\beta \delta z L \tau(D) (\overline{C}(0) - \overline{C}(L))$.

472 Substituting the advection approximation (Eq. 8) into Eq. 6,
473 we get an equation for the average suspended sediment con-
474 centration

$$\beta L \partial_x \overline{C} \approx -w_f^+ \overline{C} \quad (9)$$

475 which has the exponentially decaying solution

$$\overline{C}(x) = \overline{C}(0) \exp(-x/L_c) \quad (10)$$

476 with decay length $L_c = \beta L/w_f^+$, or $L_c = \beta L \delta z/(T w_f)$ after sub- 477
stituting w_f^+ .

478 From Eq. 6, the scaling of the decay length has the more 479
general form $L_c \propto Q/w_f$ (as can be verified using $Q \propto \delta z L/T$),
480 which is equivalent to the scaling of the decay or deposition
481 length in unidirectional turbulent suspensions⁵⁰: $L_c \propto HU/w_f \propto$
482 Q/w_f , where H is the flow depth, U is the (constant) flow
483 velocity and $Q \propto UH$ is the water discharge per unit width.

484 Finally, the boundary condition $\overline{C}(0)$ in Eq. 10 is obtained
485 numerically from Eq. 5 by averaging $C(0, t)$ over one tidal cycle,
486 which gives (see Fig. S3)

$$\overline{C}(0) = C_0 r(w_f^+) \quad (11)$$

487 with fitting function

$$r(w_f^+) = \left(1 + (1 + w_f^+)^{-1}\right)/2. \quad (12)$$

488 This function quantifies the average sediment concentration 489
of the ebb flow leaving the marsh platform. Defining $\overline{C}(0) \equiv$ 490
 $[\overline{C}_{\text{flood}}(0) + \overline{C}_{\text{ebb}}(0)]/2$, substituting Eqs. 11 and 12, and using
491 our assumption of a constant concentration at the marsh edge
492 during flood ($\overline{C}_{\text{flood}}(0) = C_0$), we get,

$$\overline{C}_{\text{ebb}}(0) = C_0 \left(2r(w_f^+) - 1\right) = C_0/(1 + w_f^+). \quad (13)$$

493 For small tidal ranges, the rescaled falling velocity diverges, 494
 $\overline{C}_{\text{ebb}}(0) \rightarrow 0$ and most of the sediment is deposited on the
495 marsh. For large tidal ranges, the opposite is true, $w_f^+ \rightarrow 0$ and
496 $\overline{C}_{\text{ebb}}(0) \rightarrow C_0$, i.e. most of the sediment leaves the march.

497 Inorganic accretion rate

498 In the absence of erosion, the net inorganic accretion rate
 499 averaged over a tidal cycle is defined as the volume of inor-
 500 ganic sediments suspended in the water column that settles
 501 on the marsh surface per unit area and unit time, and can
 502 be approximated as $A_i(x, D) = \rho_i^{-1} w_f \tau(D) \bar{C}(x)$, where ρ_i is
 503 the long-term averaged density of deposited sediments¹ and
 504 $\tau(D) \approx \pi^{-1} \arccos(1 - 2D/\delta z)$ is the average rescaled inunda-
 505 tion time. Using Eq. 10, $A_i(x, D)$ can be approximated as

$$A_i(x, D) \approx \rho_i^{-1} C_0 r(w_f^+) w_f \tau(D) \exp(-x/L_c). \quad (14)$$

506 In general, sediment transport properties (C_0 , L_c , D , $\tau(D)$, etc.)
 507 change with tidal range. However, in what follow (as within
 508 the main-text) we assume the average inorganic accretion rate
 509 can be simply calculated by Eq. 14 evaluated at a mean tidal
 510 range, denoted as δz for simplicity. When comparing to field
 511 data, δz is the mean over the measurement period, otherwise
 512 we use a representative value.

513 Simplified one-dimensional model of marsh dynamics

514 In order to calculate the response of the marsh/mud elevation,
 515 $Z(x, t) = \delta z/2 - D(x, t)$, to a rate R of RSLR, we propose a
 516 minimal model for the total accretion rate $\partial_t Z$ as function of
 517 the local elevation that describes: (i) marsh drowning, (ii)
 518 the formation of isolated ponds and (iii) the changes in the
 519 accretion rates once isolated ponds connect to the channel
 520 network. This model is used to generate the simulations shown
 521 in Fig. 5A.

522 We assume that above a critical elevation Z_c for marsh re-
 523 covery (see ‘‘Model approach’’ in the main text), marshes are
 524 widespread and both inorganic and organic accretion con-
 525 tributes to $\partial_t Z$. In that case, $\partial_t Z = A_i(x, Z, t) + A_o(D) - R$, where
 526 $A_o(D)$ is the depth-dependent organic accretion rate (by de-
 527 finition $D = \delta z/2 - Z$). We assume that for elevations below
 528 Z_c but above an arbitrary lower elevation Z_t , marshes drown
 529 ($A_o = 0$) and form isolated ponds with no net inorganic ac-
 530 cretion ($A_i = 0$). Thus, the average deepening rate of an isolate
 531 pond equals the rate of RSLR: $\partial_t Z = -R$. Finally, when the
 532 pond elevation is below Z_t , we assume ponds connect to the
 533 channel network and reach an equilibrium depth slightly lower
 534 than Z_t , and thus $\partial_t Z = 0$.

535 The minimal marsh model has the form:

$$\partial_t Z = \begin{cases} A_i(x, Z, t) + A_o(D) - R & \text{for } Z > Z_c \\ -R & \text{for } Z_t < Z \leq Z_c \\ 0 & \text{for } Z \leq Z_t \end{cases} \quad (15)$$

536 Since we are primarily interested in drowning marshes, for
 537 which $R > \max\{A_o\}$ and thus are closer to the critical elevation
 538 Z_c , we assume for simplicity a constant accretion rate A_o in the
 539 range $A_o^c \leq A_o \leq \max\{A_o\}$, where $A_o^c = A_o(D_c)$ is the organic
 540 accretion rate at the critical depth ($D_c = \delta z/2 - Z_c$).

541 The inorganic accretion rate $A_i(x, Z, t)$ is given by Eq. 14
 542 and can be written in terms of the critical accretion rate in the
 543 marsh interior, $A_i^c(L) = A_i(L, D_c)$, as:

$$A_i(x, Z, t) = A_i^c(L) \frac{\tau(Z)}{\tau(Z_c)} \exp\left(\frac{1 - \ell(x, t)}{\ell_c}\right), \quad (16)$$

544 where $\tau(Z) = \pi^{-1} \arccos(2Z/\delta z)$ is the rescaled inundation time
 545 at elevation Z , $\ell_c = \beta/w_f^+$ is the rescaled decay length $\ell_c = L_c/L$

and the function $\ell(x, t) \in [0, 1]$ is defined as the distance from
 the edge of a channel (or connected pond) rescaled such that
 $\ell = 1$ at the corresponding watershed divide (e.g. $\ell(x) = x/L$ if
 the marsh edge is at $x = 0$ and the watershed divide at $x = L$).

A further simplification is obtained by approximating
 $\pi^{-1} \arccos(x)$ by $(1 - x)/2$ in the rescaled inundation time τ ,
 which gives

$$\tau(Z) = \frac{1}{2} - \frac{Z(x, t)}{\delta z}. \quad (17)$$

Using $Z_c/\delta z = 0.15$ as the critical elevation for marshes (corre-
 sponding to $D_c = 0.35\delta z$, see Fig. 1) we get $\tau(Z_c) = 0.35$.

The function $\ell(x, t)$ in Eq. 16 generalizes the concept of the
 distance x to the marsh edge to account for the formation of
 new connected ponds. We assume that connected ponds
 change the geometry of the drainage basin and become a
 new source of both tidal water and inorganic sediment with
 concentration C_0 . As ponds get deeper than Z_t and connect to
 the channel network, we update the term $\ell(x, t)$ to reflect the
 positions x_j of the new marsh edges (defined by the condition
 $Z(x_j) = Z_t$), and corresponding watershed divides (defined
 as the midpoint between neighboring channels or connected
 ponds.)

For the numerical integration of Eqs. 15, 16 and 17, rates are
 rescaled by the drowning threshold $R_c = A_o + A_i^c(L)$, lengths are
 rescaled by the initial domain size L_0 , elevations are rescaled
 by tidal range δz and times are rescaled by $\delta z/R_c$. Since
 $A_i^c(L) = R_c - A_o$ by definition, the model has five dimensionless
 parameters: R/R_c , A_o/R_c , ℓ_c , $Z_c/\delta z$ and $Z_t/\delta z$.

For the simulations shown in Fig. 5A, we choose values
 representative of a microtidal marsh with moderate sediment
 supply: $\delta z = 1\text{m}$ and $C_0 = 50\text{g/m}^3$, with $A_o = 3\text{mm/yr}$, $w_f =$
 10^{-4}m/s and $T = 12.5\text{h}$. We thus get $A_o/R_c = 0.78$ and $\ell_c = 1/3$.
 We use a rescaled critical elevation $Z_c/\delta z = 0.15$ consistent
 with field data (Fig. 1B), and assume ponds with a depth
 around MSL connect to channels, thus $Z_t/\delta z = 0$. We change
 the rescaled RSLR rates R/R_c in the range 0.8–5. The initial
 condition is a marsh platform of rescaled elevation $Z/\delta z = 0.4$
 and unit rescaled length, limited by tidal channels at both sides.
 For the pond size distributions shown in Fig. 5B, we choose a
 10km domain size.

544 Scaling of the equilibrium pond size L_p

545 The scale invariance of spatial sediment deposition patterns
 546 leads to a similar scale invariance in the size, or diameter L_p ,
 547 of the resulting ponds. Assuming the edge of the pond, a
 548 distance $x_p = L - L_p/2$ from the channel bank, is at equilib-
 549 rium with RSLR at the critical depth D_c , then $R = A_o^c + A_i^c(x_p)$
 550 (Eq. 15). Substituting Eq. 16 with $Z(x_p) = Z_c$ and rescaled po-
 551 sition of the pond edge $\ell(x_p) = x_p/L = 1 - L_p/(2L)$, and using
 552 the definition of the drowning threshold $R_c = A_o^c + A_i^c(L)$, the
 553 rescaled equilibrium pond size is

$$\frac{L_p}{L} = 2\ell_c \ln\left(\frac{R - A_o^c}{R_c - A_o^c}\right), \quad (18)$$

544 where, $\ell_c = \beta/w_f^+ = \beta\delta z/(Tw_f)$ is the rescaled sediment con-
 545 centration decay length.

546 The rescaled equilibrium pond size (Eq. 18) has two limits:
 547 no permanent ponds ($L_p = 0$) for $R \leq R_c$, and no marshes
 548 ($L_p = 2L$) above the highest drowning threshold at marsh edge,
 549 $R \geq A_o^c + A_i^c(0) = A_o^c + (R_c - A_o^c) \exp(1/\ell_c)$ (Fig. 5A). Note that

600 this pond size is a minimum value as we assume no lateral
601 pond erosion besides marsh drowning.

602 Analysis and interpretation of inorganic accretion data

603 To only test the dependence on the distance to channel,
604 reported accretion rates A_i for Phillips Creek (Fig. 3D)
605 were depth-corrected to eliminate the scaling with the
606 flooding frequency: $A_i^* = A_i \tau(\bar{D}) / \tau(D)$, where $\tau(D) =$
607 $\pi^{-1} \arccos(1 - 2D/\delta z)$ is the approximated rescaled inundation
608 time and \bar{D} is the mean marsh depth. We couldn't perform a
609 similar correction for Norfolk (Fig. 3E) because lack of detailed
610 elevation data. However, the fact this marsh is relatively young
611 and hasn't reached a steady state elevation yet suggests the
612 noticeable exponential decay in both the 5-year average ac-
613 cretion rates and the values during individual tides is mainly
614 due to the spatial gradient of sediment distribution²¹. For the
615 Bay of Fundy, there is no obvious trend in accretion rates as
616 they were poorly correlated with both marsh elevation (for the
617 relevant range above 5.2m) and distance to channel (Fig. 3F).
618 However, this is consistent with our prediction for very large
619 tidal ranges (Eq. 2).

620 Acknowledgements

621 We acknowledge Lennert Schepers for kindly providing some
622 of the pond area data. This work was funded by the Na-
623 tional Science Foundation Coastal SEES (#1426981), GLD
624 (#1529245), CAREER (#1654374), and LTER (#1237733) pro-
625 grams. O.D.V. acknowledges the support of the Texas A&M
626 Engineering Experiment Station (TEES).

627 Author Contributions

628 Conceptualization, O.D.V, E.R.H. and M.L.K.; Methodology,
629 O.D.V; Software, O.D.V; Investigation, O.D.V; Writing—Original
630 Draft, O.D.V, E.R.H. and M.L.K.; Writing—Review & Editing,
631 O.D.V, E.R.H. and M.L.K.; Validation, O.D.V., D.J.C. and J.D.H.;
632 Funding Acquisition, M.L.K.

633 Declaration of Interests

634 The authors declare no competing interests.

635 References

- 636 1. Morris, J. T., Barber, D. C., Callaway, J. C., Chambers, R.,
637 Hagen, S. C., Hopkinson, C. S., Johnson, B. J., Megoni-
638 gal, P., Neubauer, S. C., Troxler, T. & Wigand, C. (2016).
639 Contributions of organic and inorganic matter to sediment
640 volume and accretion in tidal wetlands at steady state:
641 Sediment bulk density and ignition loss. *Earth's Futur.* **4**,
642 110–121, [10.1002/2015EF000334](https://doi.org/10.1002/2015EF000334).
- 643 2. Kirwan, M. L., Temmerman, S., Skeehan, E. E., Gun-
644 tenspergen, G. R. & Fagherazzi, S. (2016). Overestima-
645 tion of marsh vulnerability to sea level rise. *Nat. Clim.*
646 *Chang.* **6**, 253–260, [10.1038/nclimate2909](https://doi.org/10.1038/nclimate2909).
- 647 3. Marani, M., D'Alpaos, A., Lanzoni, S., Carniello, L. &
648 Rinaldo, A. (2007). Biologically-controlled multiple equi-
649 libria of tidal landforms and the fate of the Venice lagoon.
650 *Geophys. Res. Lett.* **34**, [10.1029/2007GL030178](https://doi.org/10.1029/2007GL030178).

- 651 4. Fagherazzi, S., Kirwan, M. L., Mudd, S. M., Guntensper-
652 gen, G. R., Temmerman, S., Rybczyk, J. M., Reyes, E.,
653 Craft, C. & Clough, J. (2012). Numerical models of salt
654 marsh evolution: Ecological, geomorphic, and climatic
655 factors. *Rev. Geophys.* 1–28, [10.1029/2011RG000359](https://doi.org/10.1029/2011RG000359).
- 656 5. Kolker, A. S., Kirwan, M. L., Goodbred, S. L. & Cochran,
657 J. K. (2010). Global climate changes recorded in coastal
658 wetland sediments: Empirical observations linked to the-
659 oretical predictions. *Geophys. Res. Lett.* **37**, [10.1029/
2010GL043874](https://doi.org/10.1029/2010GL043874).
- 660 6. Hill, T. D. & Anisfeld, S. C. (2015). Coastal wetland re-
661 sponse to sea level rise in Connecticut and New York.
662 *Estuarine, Coast. Shelf Sci.* **163**, 185–193, [10.1016/j.ecss.
2015.06.004](https://doi.org/10.1016/j.ecss.2015.06.004).
- 663 7. Alizad, K., Hagen, S. C., Morris, J. T., Medeiros, S. C.,
664 Bilskie, M. V. & Weishampel, J. F. (2016). Coastal wetland
665 response to sea-level rise in a fluvial estuarine system.
666 *Earth's Futur.* **4**, 483–497, [10.1002/2016EF000385](https://doi.org/10.1002/2016EF000385).
- 667 8. Alizad, K., Hagen, S. C., Medeiros, S. C., Bilskie, M. V.,
668 Morris, J. T., Balthis, L. & Buckel, C. A. (2018). Dynamic
669 responses and implications to coastal wetlands and the
670 surrounding regions under sea level rise. *PLOS ONE* **13**,
671 e0205176, [10.1371/journal.pone.0205176](https://doi.org/10.1371/journal.pone.0205176).
- 672 9. Day, J., Ibáñez, C., Scarton, F., Pont, D., Hensel, P., Day,
673 J. & Lane, R. (2011). Sustainability of Mediterranean
674 Deltaic and Lagoon Wetlands with Sea-Level Rise: The
675 Importance of River Input. *Estuaries Coasts* **34**, 483–493,
676 [10.1007/s12237-011-9390-x](https://doi.org/10.1007/s12237-011-9390-x).
- 677 10. Kirwan, M. L. & Megonigal, J. P. (2013). Tidal wetland
678 stability in the face of human impacts and sea-level rise.
679 *Nature* **504**, 53–60, [10.1038/nature12856](https://doi.org/10.1038/nature12856).
- 680 11. Kearney, M. S. (2016). Microtidal Marshes: Can These
681 Widespread and Fragile Marshes Survive Increasing Cli-
682 mate—Sea Level Variability and Human Action? *J. Coast.*
683 *Res.* **32**, 686, [10.2112/JCOASTRES-D-15-00069.1](https://doi.org/10.2112/JCOASTRES-D-15-00069.1).
- 684 12. D'Alpaos, A., Mudd, S. M. & Carniello, L. (2011). Dynamic
685 response of marshes to perturbations in suspended sedi-
686 ment concentrations and rates of relative sea level rise. *J.*
687 *Geophys. Res. Earth Surf.* **116**, [10.1029/2011JF002093](https://doi.org/10.1029/2011JF002093).
- 688 13. Kirwan, M. L., Guntenspergen, G. R., D'Alpaos, A., Morris,
689 J. T., Mudd, S. M. & Temmerman, S. (2010). Limits on
690 the adaptability of coastal marshes to rising sea level.
691 *Geophys. Res. Lett.* **37**, n/a–n/a, [10.1029/2010GL045489](https://doi.org/10.1029/2010GL045489).
- 692 14. Turner, R. E., Swenson, E. M. & Milan, C. S. Organic
693 and Inorganic Contributions to Vertical Accretion in Salt
694 Marsh Sediments. In *Concepts and Controversies in*
695 *Tidal Marsh Ecology*, 583–595, [10.1007/0-306-47534-027](https://doi.org/10.1007/0-306-47534-027)
696 (Springer, Dordrecht, 2002).
- 697 15. Nyman, J. A., Walters, R. J., Delaune, R. D. & Patrick,
698 W. H. (2006). Marsh vertical accretion via vegetative
699 growth. *Estuarine, Coast. Shelf Sci.* **69**, 370–380, [10.1016/
j.ecss.2006.05.041](https://doi.org/10.1016/j.ecss.2006.05.041).
- 700 16. Neubauer, S. C. (2008). Contributions of mineral and
701 organic components to tidal freshwater marsh accretion.
702 *Estuarine, Coast. Shelf Sci.* **78**, 78–88, [10.1016/j.ecss.2007.
11.011](https://doi.org/10.1016/j.ecss.2007.11.011).
- 703 17. Kirwan, M. L. & Guntenspergen, G. R. (2012). Feedbacks
704 between inundation, root production, and shoot growth
705
706
707
708

- in a rapidly submerging brackish marsh. *J. Ecol.* **100**, 764–770, [10.1111/j.1365-2745.2012.01957.x](https://doi.org/10.1111/j.1365-2745.2012.01957.x).
18. D’Alpaos, A. (2011). The mutual influence of biotic and abiotic components on the long-term ecomorphodynamic evolution of salt-marsh ecosystems. *Geomorphology* **126**, 269–278, [10.1016/j.geomorph.2010.04.027](https://doi.org/10.1016/j.geomorph.2010.04.027).
19. Ratliff, K. M., Braswell, A. E. & Marani, M. (2015). Spatial response of coastal marshes to increased atmospheric CO₂. *Proc. Natl. Acad. Sci.* 201516286, [10.1073/pnas.1516286112](https://doi.org/10.1073/pnas.1516286112).
20. D’Alpaos, A. & Marani, M. (2016). Reading the signatures of biologic–geomorphic feedbacks in salt-marsh landscapes. *Adv. Water Resour.* **93**, Part B, 265–275, [10.1016/j.advwatres.2015.09.004](https://doi.org/10.1016/j.advwatres.2015.09.004).
21. French, J. R. & Spencer, T. (1993). Dynamics of sedimentation in a tide-dominated backbarrier salt marsh, Norfolk, UK. *Mar. Geol.* **110**, 315–331.
22. Christiansen, T., Wiberg, P. & Milligan, T. (2000). Flow and Sediment Transport on a Tidal Salt Marsh Surface. *Estuarine, Coast. Shelf Sci.* **50**, 315–331, [10.1006/ecss.2000.0548](https://doi.org/10.1006/ecss.2000.0548).
23. Temmerman, S., Govers, G., Wartel, S. & Meire, P. (2003). Spatial and temporal factors controlling short-term sedimentation in a salt and freshwater tidal marsh, Scheldt estuary, Belgium, SW Netherlands. *Earth Surf. Process. Landforms* **28**, 739–755.
24. Reed, D. J. (1995). The response of coastal marshes to sea-level rise: Survival or submergence? *Earth Surf. Process. Landforms* **20**, 39–48, [10.1002/esp.3290200105](https://doi.org/10.1002/esp.3290200105).
25. Fagherazzi, S., Wiberg, P. L., Temmerman, S., Struyf, E., Zhao, Y. & Raymond, P. A. (2013). Fluxes of water, sediments, and biogeochemical compounds in salt marshes. *Ecol. Process.* **2**, 3, [10.1186/2192-1709-2-3](https://doi.org/10.1186/2192-1709-2-3).
26. Temmerman, S., Bouma, T. J., Govers, G., Wang, Z. B., De Vries, M. B. & Herman, P. M. J. (2005). Impact of vegetation on flow routing and sedimentation patterns: Three-dimensional modeling for a tidal marsh. *J. Geophys. Res. Earth Surf.* **110**, n/a–n/a, [10.1029/2005JF000301](https://doi.org/10.1029/2005JF000301).
27. D’Alpaos, A., Lanzoni, S., Marani, M. & Rinaldo, A. (2007). Landscape evolution in tidal embayments: Modeling the interplay of erosion, sedimentation, and vegetation dynamics. *J. Geophys. Res. Earth Surf.* **112**, F01008, [10.1029/2006JF000537](https://doi.org/10.1029/2006JF000537).
28. Da Lio Cristina, D’Alpaos Andrea & Marani Marco (2013). The secret gardener: vegetation and the emergence of biogeomorphic patterns in tidal environments. *Philos. Transactions Royal Soc. A: Math. Phys. Eng. Sci.* **371**, 20120367, [10.1098/rsta.2012.0367](https://doi.org/10.1098/rsta.2012.0367).
29. Belliard, J. P., Di Marco, N., Carniello, L. & Toffolon, M. (2016). Sediment and vegetation spatial dynamics facing sea-level rise in microtidal salt marshes: Insights from an ecogeomorphic model. *Adv. Water Resour.* **93**, 249–264, [10.1016/j.advwatres.2015.11.020](https://doi.org/10.1016/j.advwatres.2015.11.020).
30. Mudd, S. M., D’Alpaos, A. & Morris, J. T. (2010). How does vegetation affect sedimentation on tidal marshes? Investigating particle capture and hydrodynamic controls on biologically mediated sedimentation. *J. Geophys. Res.* **115**, [10.1029/2009JF001566](https://doi.org/10.1029/2009JF001566).
31. Roner, M., D’Alpaos, A., Ghinassi, M., Marani, M., Silvestri, S., Franceschinis, E. & Realdon, N. (2016). Spatial variation of salt-marsh organic and inorganic deposition and organic carbon accumulation: Inferences from the Venice lagoon, Italy. *Adv. Water Resour.* **93**, Part B, 276–287, [10.1016/j.advwatres.2015.11.011](https://doi.org/10.1016/j.advwatres.2015.11.011).
32. Ganju, N. K., Kirwan, M. L., Dickhudt, P. J., Guntenspergen, G. R., Cahoon, D. R. & Kroeger, K. D. (2015). Sediment transport-based metrics of wetland stability: Sediment Metrics of Wetland Stability. *Geophys. Res. Lett.* **42**, 7992–8000, [10.1002/2015GL065980](https://doi.org/10.1002/2015GL065980).
33. Ganju, N. K., Defne, Z., Kirwan, M. L., Fagherazzi, S., D’Alpaos, A. & Carniello, L. (2017). Spatially integrative metrics reveal hidden vulnerability of microtidal salt marshes. *Nat. Commun.* **8**, [10.1038/ncomms14156](https://doi.org/10.1038/ncomms14156).
34. Christiansen, T. *Sediment Deposition on a Tidal Salt Marsh*. Ph.D. thesis, University of Virginia, Charlottesville (1998).
35. Coleman, D. J. & Kirwan, M. L. (2019). The effect of a small vegetation dieback event on salt marsh sediment transport. *Earth Surf. Process. Landforms* **44**, 944–952, [10.1002/esp.4547](https://doi.org/10.1002/esp.4547).
36. Morris, J. T., Sundareshwar, P. V., Nietch, C. T., Kjerfve, B. & Cahoon, D. R. (2002). Responses of coastal wetlands to rising sea level. *Ecology* **83**, 2869–2877.
37. French, J. (2006). Tidal marsh sedimentation and resilience to environmental change: Exploratory modelling of tidal, sea-level and sediment supply forcing in predominantly allochthonous systems. *Mar. Geol.* **235**, 119–136, [10.1016/j.margeo.2006.10.009](https://doi.org/10.1016/j.margeo.2006.10.009).
38. Carniello, L., Defina, A. & D’Alpaos, L. (2012). Modeling sand-mud transport induced by tidal currents and wind waves in shallow microtidal basins: Application to the Venice Lagoon (Italy). *Estuarine, Coast. Shelf Sci.* **102–103**, 105–115, [10.1016/j.ecss.2012.03.016](https://doi.org/10.1016/j.ecss.2012.03.016).
39. Marani, M., Lio, C. D. & D’Alpaos, A. (2013). Vegetation engineers marsh morphology through multiple competing stable states. *Proc. Natl. Acad. Sci.* **110**, 3259–3263, [10.1073/pnas.1218327110](https://doi.org/10.1073/pnas.1218327110).
40. Mariotti, G. (2016). Revisiting salt marsh resilience to sea level rise: Are ponds responsible for permanent land loss? *J. Geophys. Res. Earth Surf.* **121**, 1391–1407, [10.1002/2016JF003900](https://doi.org/10.1002/2016JF003900).
41. Schepers, L., Kirwan, M., Guntenspergen, G. & Temmerman, S. (2017). Spatio-temporal development of vegetation die-off in a submerging coastal marsh: Spatio-temporal marsh die-off. *Limnol. Oceanogr.* **62**, 137–150, [10.1002/lno.10381](https://doi.org/10.1002/lno.10381).
42. Wilson, C. A., Hughes, Z. J., FitzGerald, D. M., Hopkinson, C. S., Valentine, V. & Kolker, A. S. (2014). Saltmarsh pool and tidal creek morphodynamics: Dynamic equilibrium of northern latitude saltmarshes? *Geomorphology* **213**, 99–115, [10.1016/j.geomorph.2014.01.002](https://doi.org/10.1016/j.geomorph.2014.01.002).
43. van Belzen, J., van de Koppel, J., Kirwan, M. L., van der Wal, D., Herman, P. M. J., Dakos, V., Kéfi, S., Scheffer, M., Guntenspergen, G. R. & Bouma, T. J. (2017). Vegetation recovery in tidal marshes reveals critical slowing down under increased inundation. *Nat. Commun.* **8**, 15811, [10.1038/ncomms15811](https://doi.org/10.1038/ncomms15811).

- 826 **44.** Rinaldo, A., Fagherazzi, S., Lanzoni, S., Marani, M. & 884
827 Dietrich, W. E. (1999). Tidal networks 2. Watershed de- 885
828 lineation and comparative network morphology. *Water*
829 *Resour. Res.* **35**, 3905–3917.
- 830 **45.** Belliard, J.-P., Toffolon, M., Carniello, L. & D’Alpaos, A. 886
831 (2015). An ecogeomorphic model of tidal channel initiation 887
832 and elaboration in progressive marsh accretional contexts. 888
833 *J. Geophys. Res. Earth Surf.* **120**, 1040–1064, [10.1002/](https://doi.org/10.1002/2015JF003445)
834 [2015JF003445](https://doi.org/10.1002/2015JF003445).
- 835 **46.** Wang, C. & Temmerman, S. (2013). Does biogeomorphic 889
836 feedback lead to abrupt shifts between alternative land- 890
837 scape states?: An empirical study on intertidal flats and 891
838 marshes. *J. Geophys. Res. Earth Surf.* **118**, 229–240, 892
839 [10.1029/2012JF002474](https://doi.org/10.1029/2012JF002474).
- 840 **47.** Defina, a., Carniello, L., Fagherazzi, S. & D’Alpaos, L. 893
841 (2007). Self-organization of shallow basins in tidal flats 894
842 and salt marshes. *J. Geophys. Res.* **112**, F03001–F03001, 895
843 [10.1029/2006JF000550](https://doi.org/10.1029/2006JF000550).
- 844 **48.** Fagherazzi, S., Carniello, L., D’Alpaos, L. & Defina, A. 896
845 (2006). Critical bifurcation of shallow microtidal landforms 897
846 in tidal flats and salt marshes. *Proc. Natl. Acad. Sci. United*
847 *States Am.* **103**, 8337–41, [10.1073/pnas.0508379103](https://doi.org/10.1073/pnas.0508379103).
- 848 **49.** Wang, C., Schepers, L., Kirwan, M. L., Belluco, E., 898
849 D’Alpaos, A., Wang, Q., Yin, S. & Temmerman, S. 899
850 (2021). Different coastal marsh sites reflect similar to- 900
851 pographic conditions under which bare patches and 901
852 vegetation recovery occur. *Earth Surf. Dyn.* **9**, 71–88, 902
853 [10.5194/esurf-9-71-2021](https://doi.org/10.5194/esurf-9-71-2021).
- 854 **50.** Claudin, P., Charru, F. & Andreotti, B. (2011). Transport 903
855 relaxation time and length scales in turbulent suspensions. 904
856 *J. Fluid Mech.* **671**, 491–506, [10.1017/S0022112010005823](https://doi.org/10.1017/S0022112010005823).
- 857 **51.** Coleman, D. J., Ganju, N. K. & Kirwan, M. L. (2020). 905
858 Sediment delivery to a tidal marsh platform is minimized 906
859 by source decoupling and flux convergence. *J. Geophys.*
860 *Res. Surf. (in press)* [10.1029/2020JF005558](https://doi.org/10.1029/2020JF005558).
- 861 **52.** van Proosdij, D., Davidson-Arnott, R. G. & Ollerhead, J. 907
862 (2006). Controls on spatial patterns of sediment depo- 908
863 sition across a macro-tidal salt marsh surface over sin- 909
864 gle tidal cycles. *Estuarine, Coast. Shelf Sci.* **69**, 64–86, 910
865 [10.1016/j.ecss.2006.04.022](https://doi.org/10.1016/j.ecss.2006.04.022).
- 866 **53.** Mariotti, G., Kearney, W. & Fagherazzi, S. (2016). Soil 911
867 creep in salt marshes. *Geology* **G37708.1**, [10.1130/](https://doi.org/10.1130/G37708.1)
868 [G37708.1](https://doi.org/10.1130/G37708.1).
- 869 **54.** Newman, M. (2005). Power laws, pareto distributions 912
870 and zipf’s law. *Contemp. Phys.* **46**, 323–351, [10.1080/](https://doi.org/10.1080/00107510500052444)
871 [00107510500052444](https://doi.org/10.1080/00107510500052444).
- 872 **55.** Himmelstein, J. D. *Mechanisms of Pond Expansion on the*
873 *Saltmarshes of the Blackwater National Wildlife Refuge,*
874 *Maryland.* Master’s thesis, The College of William and
875 Mary (2018).
- 876 **56.** Ortiz, A. C., Roy, S. & Edmonds, D. A. (2017). Land loss by 913
877 pond expansion on the mississippi river delta plain. *Geo-*
878 *phys. Res. Lett.* **44**, 3635–3642, [10.1002/2017GL073079](https://doi.org/10.1002/2017GL073079).
- 879 **57.** Stevenson, J. C., Kearney, M. S. & Pendleton, E. C. (1985).
880 Sedimentation and erosion in a Chesapeake Bay brackish
881 marsh system. *Mar. Geol.* **67**, 213–235.
- 882 **58.** Törnqvist, T. E., Jankowski, K. L., Li, Y.-X. & González,
883 J. L. (2020). Tipping points of Mississippi Delta marshes
due to accelerated sea-level rise. *Sci. Adv.* **6**, eaaz5512,
[10.1126/sciadv.aaz5512](https://doi.org/10.1126/sciadv.aaz5512).
- 59.** Reef, R., Spencer, T., Möller, I., Lovelock, C. E., Christie,
E. K., Mclvor, A. L., Evans, B. R. & Tempest, J. A. (2017).
The effects of elevated CO₂ and eutrophication on surface
elevation gain in a European salt marsh. *Glob. Chang.*
Biol. **23**, 881–890, [10.1111/gcb.13396](https://doi.org/10.1111/gcb.13396).
- 60.** DeLaune, R. D., Whitcomb, J. H., Patrick, W. H., Pardue,
J. H. & Pezeshki, S. R. (1989). Accretion and canal im-
pacts in a rapidly subsiding wetland. I. 137 Cs and 210
Pb techniques. *Estuaries Coasts* **12**, 247–259.
- 61.** Burdick, D. M., Moore, G. E., Adamowicz, S. C., Wilson,
G. M. & Peter, C. R. (2019). Mitigating the Legacy Effects
of Ditching in a New England Salt Marsh. *Estuaries Coasts*
[10.1007/s12237-019-00656-5](https://doi.org/10.1007/s12237-019-00656-5).
- 62.** Mariotti, G. & Fagherazzi, S. (2013). Critical width of tidal
flats triggers marsh collapse in the absence of sea-level
rise. *Proc. Natl. Acad. Sci.* **110**, 5353–5356, [10.1073/pnas.](https://doi.org/10.1073/pnas.1219600110)
[1219600110](https://doi.org/10.1073/pnas.1219600110).
- 63.** Schuerch, M., Spencer, T., Temmerman, S., Kirwan,
M. L., Wolff, C., Lincke, D., McOwen, C. J., Pickering,
M. D., Reef, R., Vafeidis, A. T., Hinkel, J., Nicholls,
R. J. & Brown, S. (2018). Future response of global
coastal wetlands to sea-level rise. *Nature* **561**, 231–234,
[10.1038/s41586-018-0476-5](https://doi.org/10.1038/s41586-018-0476-5).
- 64.** Temmerman, S., Govers, G., Wartel, S. & Meire, P.
(2004). Modelling estuarine variations in tidal marsh
sedimentation: response to changing sea level and sus-
pended sediment concentrations. *Mar. Geol.* **212**, 1–19,
[10.1016/j.margeo.2004.10.021](https://doi.org/10.1016/j.margeo.2004.10.021).

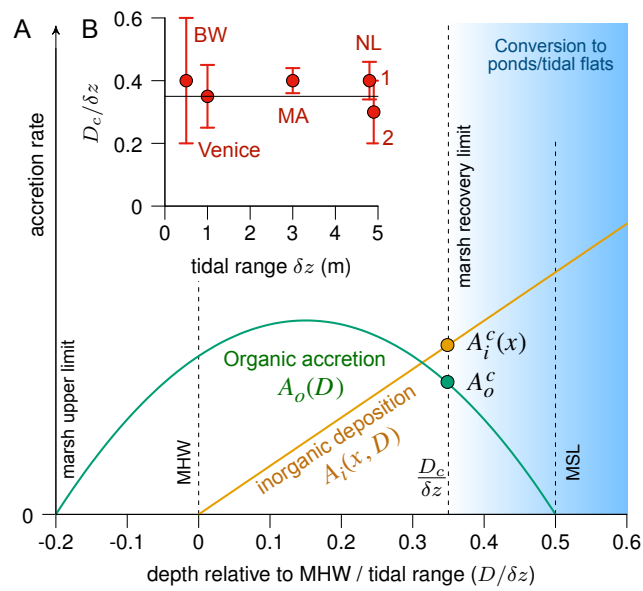


Figure 1. Critical depth for marsh recovery. (A) Sketch of the organic (A_o) and inorganic (A_i) accretion rates on a marsh platform as function of the local water depth (D) relative to mean high water level (MHW) and rescaled by tidal range δz . Accretion rates (A_i^c and A_o^c) at the critical depth for marsh recovery (D_c) determine the marsh response to sea level rise, where $A_i^c(x)$ is in general function of the distance x to sediment sources. (B) Estimated values for the rescaled critical depth ($D_c/\delta z$) at different locations suggested by field data: Blackwater, MD (BW)⁴⁹; Plum Island, MA (MA)⁴²; Venice, Italy (general^{47,48} and for San Felice marshes⁴⁹); Hallegat and Paulina marshes, NL (NL 1)⁴³; and Western Scheldt estuary, NL (NL 2)⁴⁶ (see Table S1 for details).

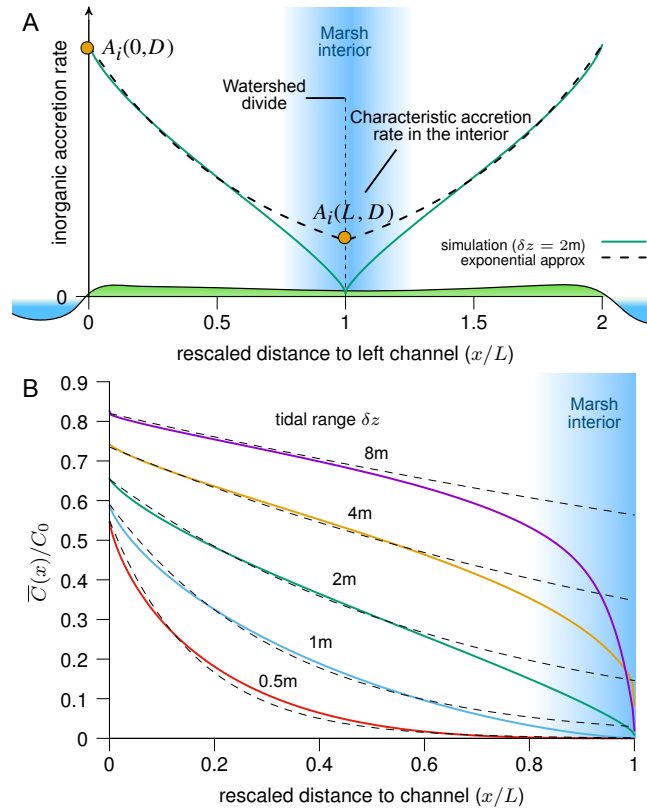


Figure 2. Spatial decay of sediment concentration and scaling with tidal range. Simulation and exponential approximation of the decay of the average sediment concentration \bar{C} with the rescaled distance from channel x/L , where L is the length of the drainage basin. For illustration purposes we show in (A) the inorganic accretion rate for a constant marsh depth D —such that $A_i(x, D) \propto \bar{C}(x)$ —where $A_i(0, D)$ is the accretion rate at the marsh edge and $A_i(L, D)$ is the characteristic accretion rate in the marsh interior. (B) Rescaled \bar{C}/C_0 simulated for simplicity for constant marsh depth and varying tidal range δz (solid lines). The effective sediment falling velocity is $w_f = 10^{-4}$ m/s and the tidal period is $T = 12.5$ h. Dashed lines show the exponential approximation $\bar{C}(x) = \bar{C}(0)e^{-x/L_c}$ with L_c given by Eq. 2.

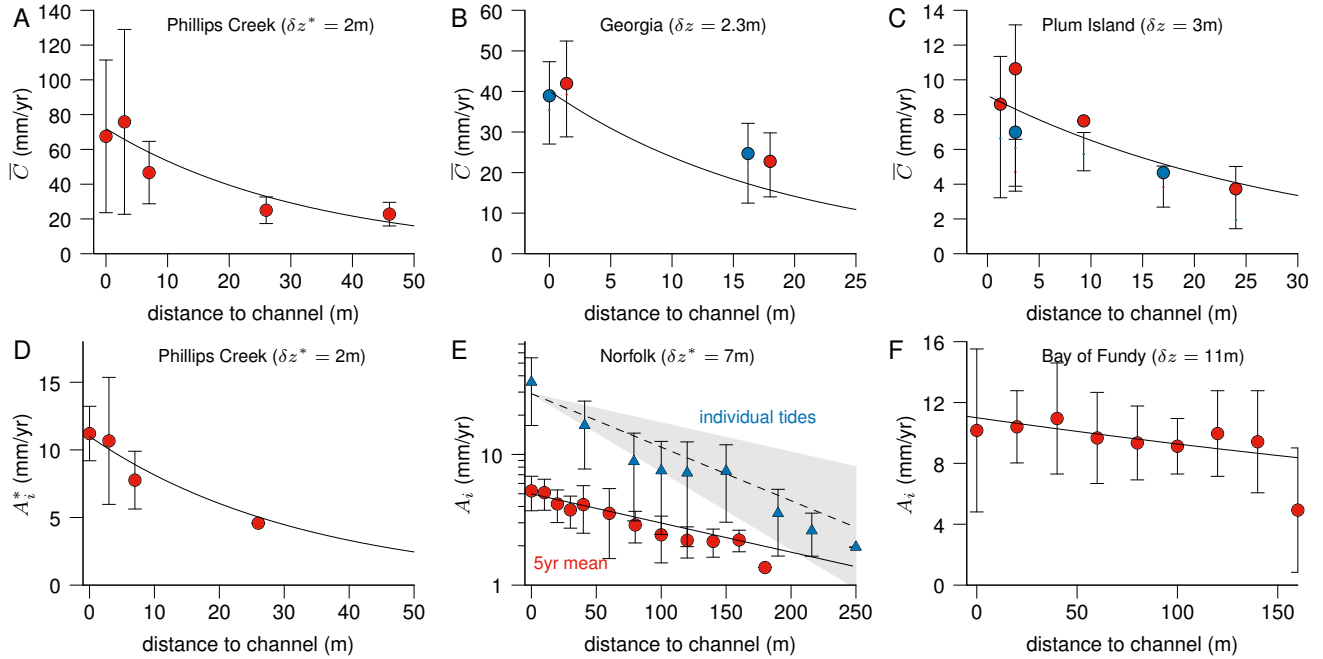


Figure 3. Validation of the exponential decay of sediment concentration and inorganic accretion. Proposed exponential decay (lines) compared to measurements of averaged sediment concentration \bar{C} (A³⁴, B³⁵ and C⁵¹) and inorganic accretion rate A_i (D³⁴, E²¹ and F⁵²) (symbols). A_i^* is the depth-corrected accretion rate (see Experimental Procedures for more information). The scaling of the decay length is obtained from the model as $L_c = 1.5L\delta z/(Tw_f)$ (e.g. Eq. 2), where δz is the tidal range, T is tidal period and w_f is the effective sediment falling velocity. In all cases L is taken as the maximum distance to a channel reported in the data, δz (δz^*) is the reported tidal range (average/typical tidal range during the measurement period), and we use the generic value $w_f = 10^{-4}\text{m/s}$ ^{3,22,64} unless stated otherwise. Values of $\bar{C}(0)$ and $A_i(0)$ were fitted to data. Mass accretion rate data was converted to volume accretion rate using an effective density of inorganic sediments deposited in the marsh $\rho_i \approx 2\text{g/cm}^3$ ¹. All symbols correspond to the average of reported values. Error bars in (A),(D) and (F) represent the standard deviation of the measurements, whereas in (B) and (C) represent the 25th and 75th percentiles. Error bars in (E) represent either the standard deviation (5-year mean data, circles) or the range (individual-tide data, triangles) of reported data. Colors in (B) and (C) correspond to different measurement periods. In (A), \bar{C} is calculated as the mean of the reported maximum concentrations measured during flood and ebb. In (E), we assume $w_f = 3 \times 10^{-4}\text{m/s}$, which is the lowest value of the reported range of settling velocities ($w_f = 3 - 8 \times 10^{-4}\text{m/s}$) to fit the long-term measurements (solid line), whereas we use the average value, $w_f = (5.5 \pm 2.5) \times 10^{-4}\text{m/s}$, for measurements during single tides (dashed line and shaded area). In both cases the effective tidal range $\delta z^* = 7\text{m}$ is the average of the reported range 6 – 8m²¹.

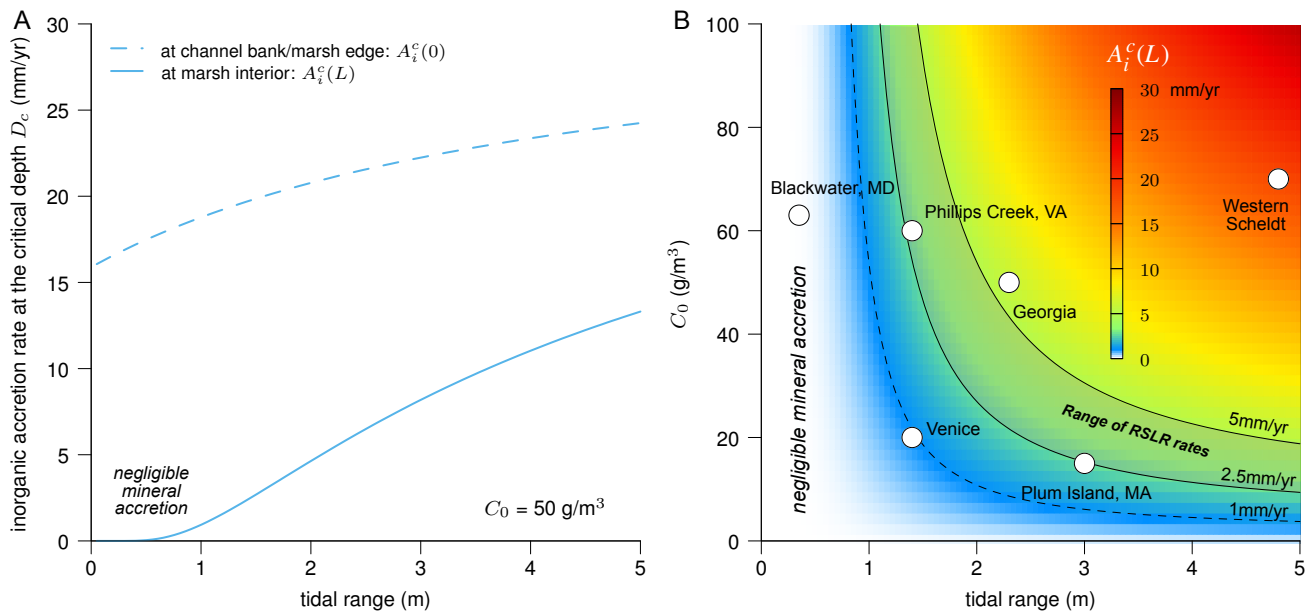


Figure 4. Predictions of critical inorganic accretion rates. (A) Inorganic accretion rates at the critical depth D_c evaluated at the marsh edge and marsh interior ($A_i^c(0)$ and $A_i^c(L)$, respectively) as function of tidal ranges for an average suspended sediment concentration at the channel bank of $C_0 = 50 \text{ g/m}^3$. We use $w_f = 10^{-4} \text{ m/s}$, which is within commonly reported ranges^{3,22,64} and $\rho_i = 2 \text{ g/cm}^3$, obtained from a meta-analysis of bulk density measurements in global marshes¹. (B) Color map of the critical inorganic accretion rate at the marsh interior $A_i^c(L)$ as function of tidal range and average SSC at the channel bank (C_0). Black lines separate regions with low inorganic deposition in the marsh interior ($A_i^c(L) < 1 \text{ mm/yr}$, dashed line) and with inorganic deposition lower than a common range of global rates of RSLR ($A_i^c(L) < 2.5 - 5 \text{ mm/yr}$, solid lines). Superimposed data: Venice, Italy³; Western Scheldt, NL⁶⁴; from USA: Blackwater, MD³³; Plum Island, MA^{42,51}; Phillips Creek, VA^{22,34}; Georgia³⁵.

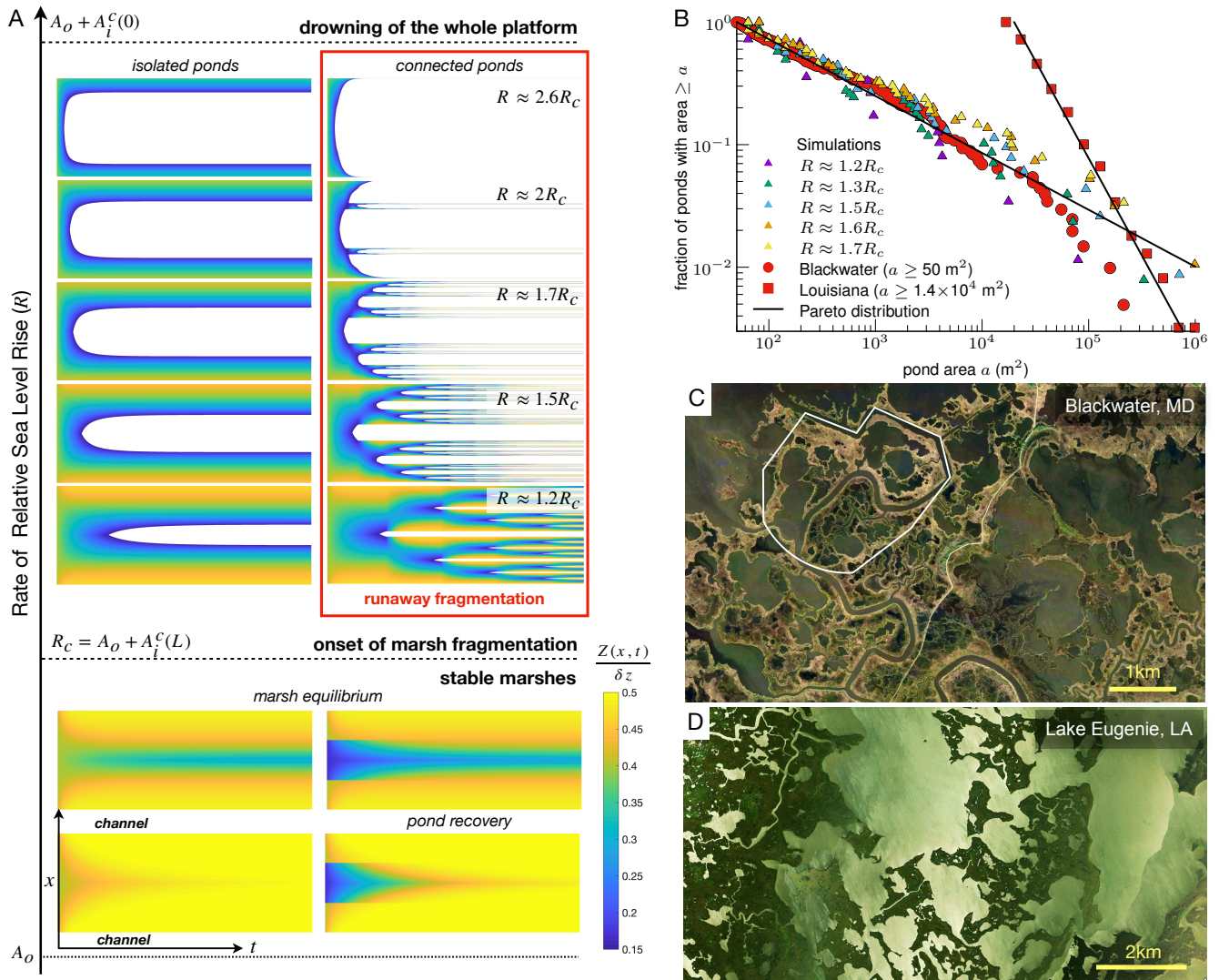


Figure 5. Marsh equilibrium states and runaway marsh fragmentation. (A) One-dimensional spatio-temporal plots of simulated marsh elevation $Z(x,t)$ (in color) for different rates R of RSLR starting from a flat marsh platform flanked by channels on both sides (see Methods for model description and parameters). For each rectangle, x runs vertically from channel to channel and t runs from left to right (see bottom left illustration). Elevations below the critical value $Z_c/\delta z = 0.15$ (corresponding to $D_c/\delta z = 0.35$) are shown in white and represent ponds. For $R < R_c$, shallow ponds can recover (bottom center) and marshes reach a non-flat equilibrium state. For $R > R_c$, marsh drowns and form ponds. If those ponds remain isolated, the marsh eventually reaches equilibrium. Otherwise, a self-similar mechanism of pond formation and basin reduction leads to a runaway marsh fragmentation. (B) Exceedance probability distribution of pond areas in Blackwater, MD (representing ponds larger than $50m^2$ within the white region in (C), see⁵⁵ for details on data acquisition, data available in Table S2) and Louisiana (reported ponds larger than $1.4 \times 10^4 m^2$ obtained from 1982-1985 composite satellite images⁵⁶). The distribution of simulated ponds (A) (with pond area defined as the square of its length) is shown for comparison. The distribution of pond area is consistent with a Pareto (power-law) distribution (linear fits), with power 1.46 for Blackwater, 2.6 for Louisiana and ~ 1.5 for the simulations. (C-D) Examples of apparently self-similar patterns from marshes in Blackwater, MD and around Lake Eugenie, Louisiana.

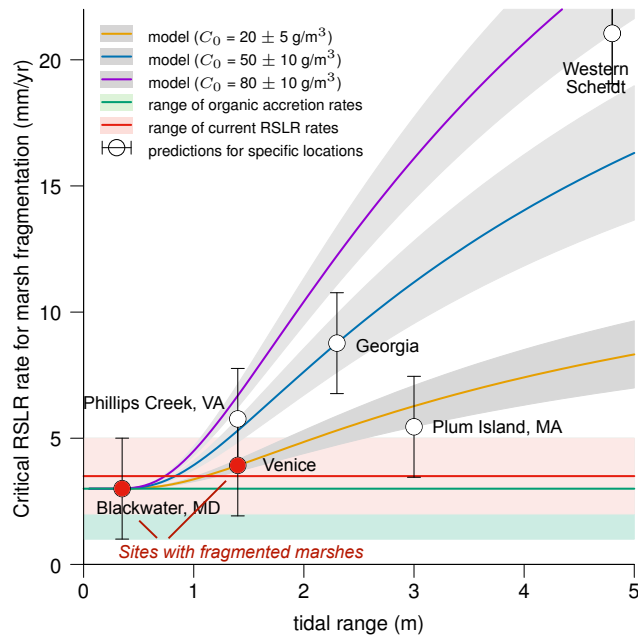


Figure 6. Threshold rates for runaway marsh fragmentation. Lines are predicted thresholds for marsh fragmentation ($R_c = A_o^c + A_i^c(L)$) as function of tidal range, for different values of the average suspended sediment concentration at the channel bank C_0 representing typical low, mid and high sediment supply conditions (see Fig. 4B). We use $w_f = 10^{-4}$ m/s and $\rho_i = 2$ g/cm³ for the calculation of the critical inorganic accretion $A_i^c(L)$ (as in Fig. 4), and assume an organic accretion rate $A_o^c = 3$ mm/yr, consistent with a meta-analysis of field data (Fig. S5 and Supplemental Experimental Procedures). Symbols represent predictions for specific locations including Blackwater, MD; Plum Island, MA; Phillips Creek, VA and Georgia (we use values shown in Fig. 4B). Current RSLR rates for those locations are in the range 3.5 ± 1.5 mm/yr (red line and shaded area). Organic accretion rates in salt marshes are in the range 3.0 ± 2.0 mm/yr (green line, shaded area and error-bars, see Fig. S5 and Supplemental Experimental Procedures).

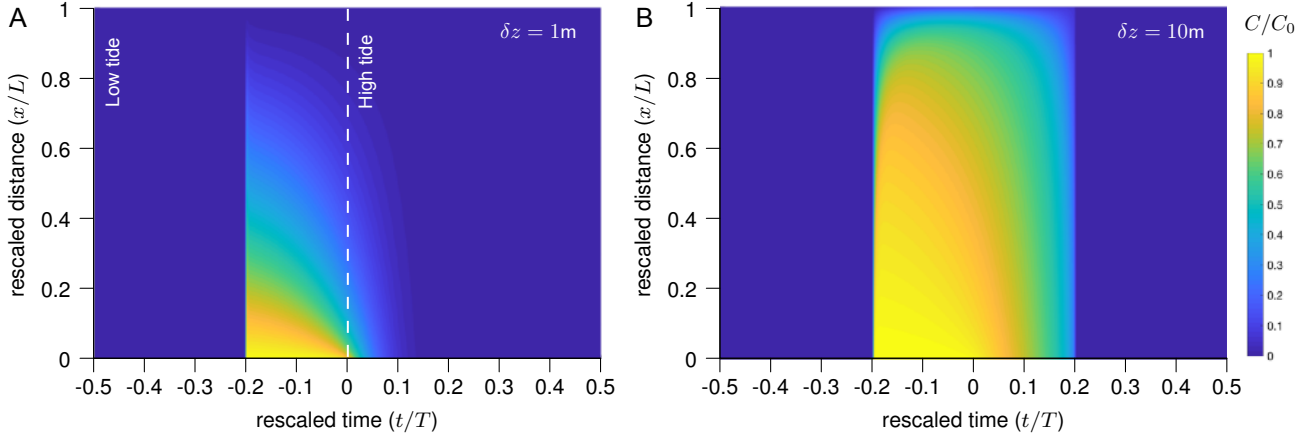


Figure S 1. Numerical solution of the rescaled depth-averaged sediment concentration C/C_0 over a flat marsh surface at a critical elevation $Z_c = 0.15\delta z$ (relative to mean sea level with tidal range δz) for two different rescaled effective falling velocity $w_f^+ = w_f T / \delta z$: $w_f^+ = 4.5$ (A) and $w_f^+ = 0.45$ (B). Time is rescaled by tidal period $T = 12.5\text{h}$, and length by the distance L to marsh edge. For $w_f = 10^{-4}\text{m/s}$, the corresponding tidal range δz is 1m (A) and 10m (B).

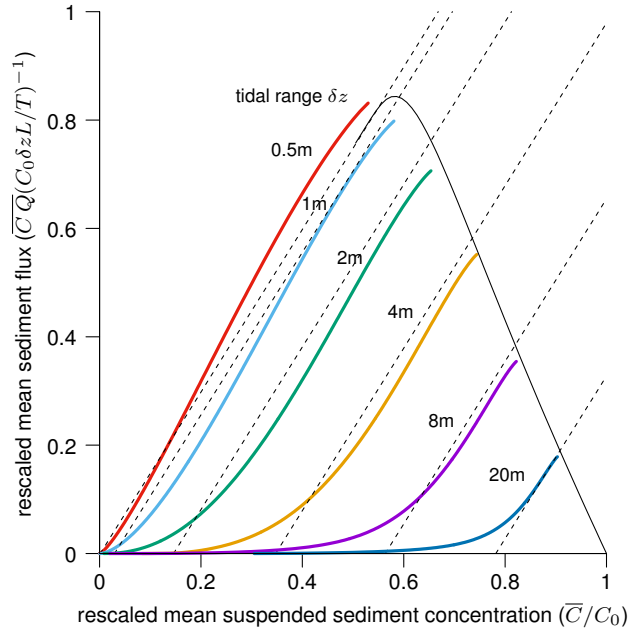


Figure S 2. Correlation between the rescaled depth-integrated sediment flux $\overline{CQ}^+ = \overline{CQ} / (C_0 \delta z L T^{-1})$ and the rescaled depth-averaged sediment concentration $\overline{C}^+ = \overline{C} / C_0$, both averaged over times of positive water depths, for different rescaled effective falling velocity $w_f^+ = w_f T / \delta z$ (parametrized by a variable tidal range δz for constant w_f). Dashed lines show the linear approximation $\overline{CQ}^+ \approx \beta [\overline{C}^+ - \overline{C}^+(L)]$ with fitting constant $\beta = 1.5$ and where $\overline{C}^+(L) = \overline{C}^+(0) e^{-w_f^+ / \beta}$ is the rescaled concentration at the watershed divide $x = L$. Solid lines show the approximated maximum rescaled average sediment flux at marsh edge ($x = 0$), given by the relation $\overline{CQ}^+(0) = \beta [\overline{C}^+(0) - \overline{C}^+(L)]$, where both $\overline{C}^+(0)$ and $\overline{C}^+(L)$ are function of tidal range via the rescaled falling velocity w_f^+ (See Fig. S3). Simulation data is shown only for the critical elevation $Z_c = 0.15\delta z$, but a similar result is obtained for any other elevation.

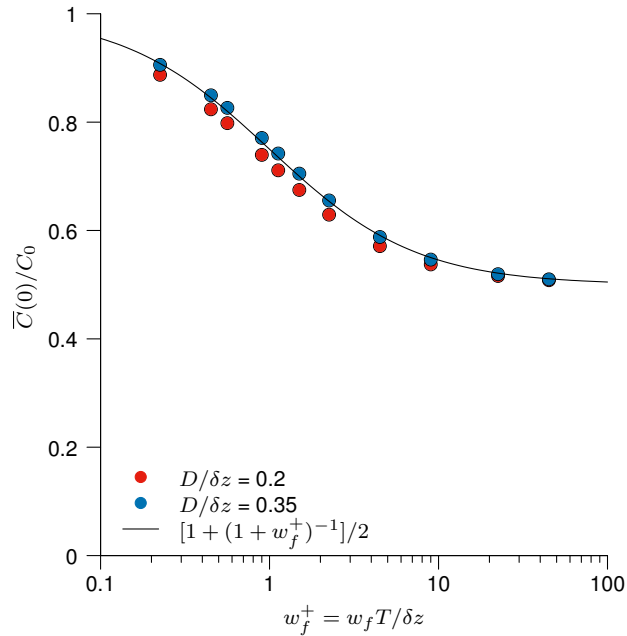


Figure S 3. The depth-averaged sediment concentration at marsh edge $\bar{C}(0)$, averaged over times with positive water depth, depends weakly on the rescaled marsh depth and has the form $\bar{C}(0) = C_0 r(w_f^+)$. The solid line shows the fitted function $r(w_f^+) = \left(1 + (1 + w_f^+)^{-1}\right) / 2$.

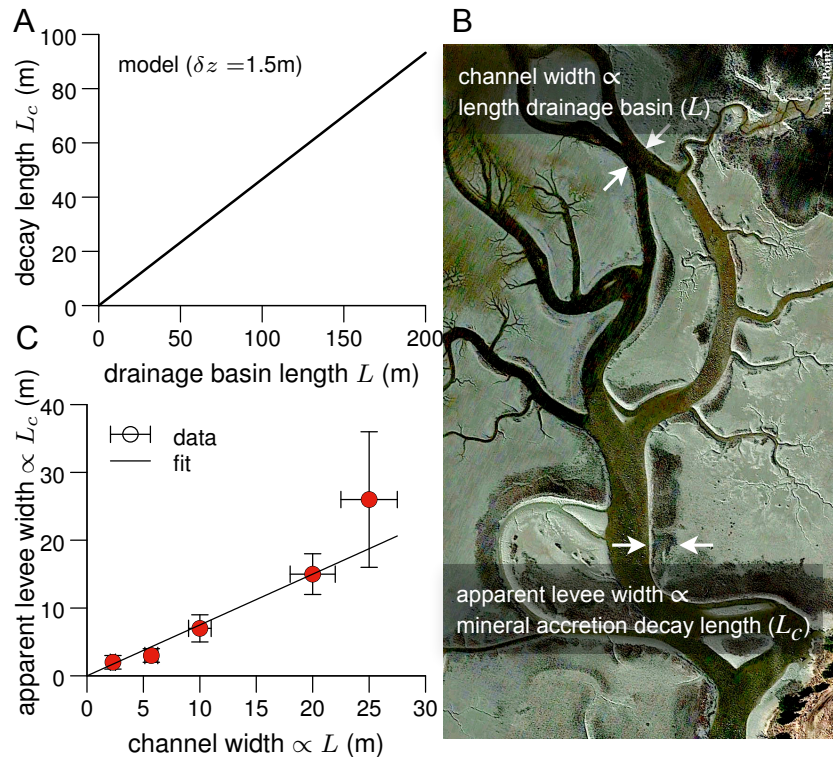


Figure S 4. Evidence of the scale invariance of inorganic deposition. (A) Scaling of the decay length L_c and the drainage basin length L predicted by the analytical model. (B) Tidal channel network in Phillips Creek, VA, USA, showing the apparent width of the levees (darker areas surrounding the channels) increasing with channel width, which suggests sediment deposits in a wider region for larger tidal flows. (C) Linear scaling obtained from the analysis of (B).

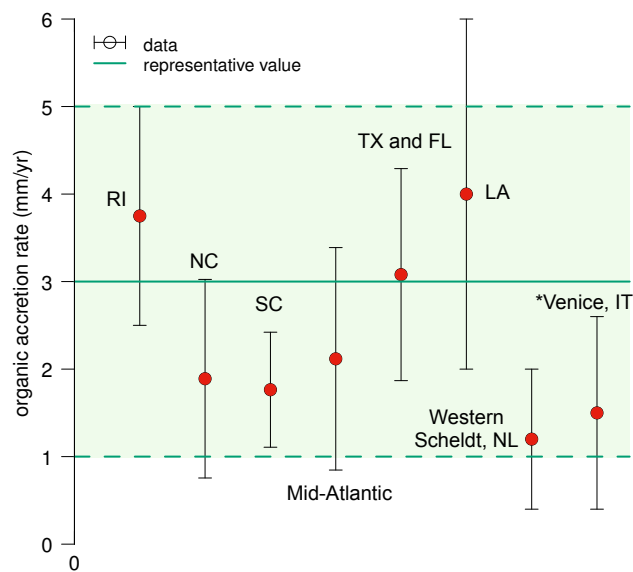


Figure S 5. Approximate range of organic accretion rates. Organic accretion rates estimated from field data are within 1 – 5 mm/yr (shadow area). Solid line shows a theoretical maximum for salt marshes¹ (representative value). Field data: Rhodes Island (RI)²; North Carolina (NC)³; South Carolina (SC)³; US Mid-Atlantic average³; Texas and Florida (TX & FL)³; Louisiana (LA)⁴; Western Scheldt, NL⁵; Venice, Italy (see Supplemental Experimental Procedures for details).

<i>Location</i>	<i>tidal range</i> δz (m)	$D_c/\delta z$	<i>Reference</i>
Blackwater, MD	0.5	0.4 ± 0.2	$D_c = \delta z/2 - Z_c \approx 0.2 \pm 0.1$ m, where $Z \approx 0.05 \pm 0.1$ m is the cross-over elevation between bare patches and vegetated ones, ⁶ . The uncertainty is approximated by the difference between the typical elevation of bare patches and vegetated areas ⁶ .
San Felice, Venice	1.0	0.35 ± 0.1	$D_c = \delta z/2 - Z_c \approx 0.35 \pm 0.1$ m, where $Z_c \approx 0.15 \pm 0.1$ m is the cross-over elevation between connected bare patches and vegetated ones ⁶ . This choice is consistent with the elevation above which marshes are generally found in the Venice lagoon, in the range 0.1-0.2m ^{7,8} . The uncertainty is approximated by the difference between the typical elevation of connected bare patches and vegetated areas ⁶ .
Plum Island, MA	3	0.40 ± 0.04	$D_c = \delta z/2 - Z_c \approx 1.2$ m, where $Z_c = 0.31$ m is the elevation (above MSL) of the lowest-elevation bare pool reported ⁹ (Duncan's pool, site R-20 in Morris Island). The uncertainty is the difference in elevation between Duncan's pool and the next low-elevation revegetating pool ($Z = 0.42$ m above MSL, site RRP-2 in Law's Point ⁹). Thus $\Delta D_c = \Delta Z_c = 0.1$ m.
Hallegat and Paulina marshes, NL	4.8	0.40 ± 0.06	Marsh recovery characterized by a critical value of average rescaled inundation time, $\tau_c = 0.44 \pm 0.02$ ¹⁰ . Assuming a constant tidal range, the rescaled inundation time $\tau(D)$ at a depth D can be written as $\tau(D) \approx \pi^{-1} \arccos(1 - 2D/\delta z)$. Therefore, the rescaled critical depth is $D_c/\delta z = 0.5(1 - \cos(\pi\tau_c)) \approx 0.40 \pm 0.03$. We double the uncertainty to account for a broader region (depth) of marsh vulnerability ¹⁰ .
Western Scheldt, NL	4.9	0.3 ± 0.1	Estimation from the reported occurrence probability of pioneer plants patches ¹¹ , which is between 0-1% for depths in the range 1-2m ¹¹ . Thus $D_c = 1.5 \pm 0.5$ m.

Table S 1. Estimation of the rescaled critical depth for marsh recovery ($D_c/\delta z$) shown in Fig. 1B. By definition, $Z_c = \delta z/2 - D_c$ is the critical elevation relative to MSL.

#	A	#	A	#	A	#	A	#	A (m ²)
1	50	51	89	101	211	151	1301	201	158637
2	52	52	89	102	221	152	1314	202	212723
3	52	53	91	103	222	153	1360	203	230824
4	54	54	92	104	223	154	1367		
5	55	55	92	105	223	155	1370		
6	55	56	92	106	227	156	1470		
7	56	57	94	107	236	157	1524		
8	56	58	100	108	248	158	1605		
9	56	59	101	109	250	159	1679		
10	57	60	106	110	254	160	1699		
11	57	61	106	111	268	161	1820		
12	57	62	108	112	272	162	2137		
13	59	63	109	113	276	163	2510		
14	59	64	110	114	289	164	2519		
15	59	65	114	115	318	165	2554		
16	60	66	114	116	320	166	2998		
17	60	67	115	117	326	167	3134		
18	61	68	119	118	329	168	3300		
19	61	69	122	119	387	169	3435		
20	64	70	123	120	393	170	3508		
21	64	71	125	121	415	171	3656		
22	64	72	129	122	428	172	3695		
23	64	73	130	123	429	173	3730		
24	65	74	130	124	447	174	4071		
25	65	75	133	125	449	175	4174		
26	65	76	135	126	452	176	4303		
27	67	77	135	127	453	177	4335		
28	67	78	135	128	541	178	4384		
29	69	79	139	129	544	179	4428		
30	70	80	139	130	558	180	4714		
31	70	81	140	131	599	181	5514		
32	71	82	140	132	608	182	6331		
33	71	83	142	133	612	183	6537		
34	73	84	144	134	614	184	6551		
35	73	85	144	135	678	185	7713		
36	74	86	149	136	720	186	8132		
37	74	87	152	137	772	187	9022		
38	74	88	156	138	844	188	9325		
39	74	89	161	139	856	189	9986		
40	75	90	163	140	907	190	13973		
41	76	91	166	141	912	191	22799		
42	77	92	169	142	957	192	29843		
43	79	93	181	143	967	193	30100		
44	80	94	184	144	976	194	34837		
45	81	95	192	145	1097	195	38968		
46	82	96	195	146	1135	196	40827		
47	82	97	198	147	1137	197	55439		
48	85	98	206	148	1188	198	70379		
49	85	99	208	149	1249	199	70465		
50	88	100	209	150	1285	200	89557		

Table S 2. List of measured pond areas (A in m^2) of ponds above $50m^2$ from a 2010 aerial image of Blackwater marshes (MD)¹² (see location of the selected region in Fig. 5C). Data used in Fig. 5B.

Supplemental Experimental Procedures

Organic accretion rates

For some locations in USA (North and South Carolina, Mid-Atlantic and Texas & Florida) we used the data compilation from³, which reports the total accretion rate range (min and max values) and the slope (cm^3g^{-1}) of the linear regression between organic mass accretion rates (defined as the dependent variable, $\text{g cm}^{-3}\text{yr}^{-1}$) and total accretion rates (defined as the independent variable, cm yr^{-1}). We then obtain min and max values for organic mass accretion rates and convert them from mass to volume using an effective density of deposited organic matter: $\rho_o = 0.085 \text{ g/cm}^3$, obtained from a meta-analysis of bulk density measurements in global marshes¹. For Rhodes Island, US, we use reported values of organic mass accretion rates² converted to volume using ρ_o . We did the same for some marshes in Louisiana, US⁴. We also used reported values of organic accretion rates (mm/yr) for some locations in the Scheldt estuary, NL⁵. For Venice, we estimate organic accretion rates from reported total marsh accretion rates¹³, using the average bulk density $\approx 1 \text{ g/cm}^3$ ¹⁴ and the effective values for the density of organic and inorganic deposited sediments $\rho_i = 2 \text{ g/cm}^3$ and $\rho_o = 0.085 \text{ g/cm}^3$ respectively¹. The organic accretion rate data is shown in Fig. S5.

Supplemental References

1. Morris, J. T., Barber, D. C., Callaway, J. C., Chambers, R., Hagen, S. C., Hopkinson, C. S., Johnson, B. J., Megonigal, P., Neubauer, S. C., Troxler, T. & Wigand, C. (2016). Contributions of organic and inorganic matter to sediment volume and accretion in tidal wetlands at steady state: Sediment bulk density and ignition loss. *Earth's Futur.* **4**, 110–121, [10.1002/2015EF000334](https://doi.org/10.1002/2015EF000334).
2. Bricker-Urso, S., Nixon, S. W., Cochran, J. K., Hirschberg, D. J. & Hunt, C. (1989). Accretion rates and sediment accumulation in Rhode Island salt marshes. *Estuaries* **12**, 300–317, [10.2307/1351908](https://doi.org/10.2307/1351908).
3. Turner, R. E., Swenson, E. M. & Milan, C. S. Organic and Inorganic Contributions to Vertical Accretion in Salt Marsh Sediments. In *Concepts and Controversies in Tidal Marsh Ecology*, 583–595, [10.1007/0-306-47534-027](https://doi.org/10.1007/0-306-47534-027) (Springer, Dordrecht, 2002).
4. DeLaune, R. D., Whitcomb, J. H., Patrick, W. H., Pardue, J. H. & Pezeshki, S. R. (1989). Accretion and canal impacts in a rapidly subsiding wetland. I. 137 Cs and 210 Pb techniques. *Estuaries Coasts* **12**, 247–259.
5. Temmerman, S., Govers, G., Wartel, S. & Meire, P. (2004). Modelling estuarine variations in tidal marsh sedimentation: response to changing sea level and suspended sediment concentrations. *Mar. Geol.* **212**, 1–19, [10.1016/j.margeo.2004.10.021](https://doi.org/10.1016/j.margeo.2004.10.021).
6. Wang, C., Schepers, L., Kirwan, M. L., Belluco, E., D'Alpaos, A., Wang, Q., Yin, S. & Temmerman, S. (2021). Different coastal marsh sites reflect similar topographic conditions under which bare patches and vegetation recovery occur. *Earth Surf. Dyn.* **9**, 71–88, [10.5194/esurf-9-71-2021](https://doi.org/10.5194/esurf-9-71-2021).
7. Fagherazzi, S., Carniello, L., D'Alpaos, L. & Defina, A. (2006). Critical bifurcation of shallow microtidal landforms in tidal flats and salt marshes. *Proc. Natl. Acad. Sci. United States Am.* **103**, 8337–41, [10.1073/pnas.0508379103](https://doi.org/10.1073/pnas.0508379103).
8. Defina, a., Carniello, L., Fagherazzi, S. & D'Alpaos, L. (2007). Self-organization of shallow basins in tidal flats and salt marshes. *J. Geophys. Res.* **112**, F03001–F03001, [10.1029/2006JF000550](https://doi.org/10.1029/2006JF000550).
9. Wilson, C. A., Hughes, Z. J., FitzGerald, D. M., Hopkinson, C. S., Valentine, V. & Kolker, A. S. (2014). Saltmarsh pool and tidal creek morphodynamics: Dynamic equilibrium of northern latitude saltmarshes? *Geomorphology* **213**, 99–115, [10.1016/j.geomorph.2014.01.002](https://doi.org/10.1016/j.geomorph.2014.01.002).
10. van Belzen, J., van de Koppel, J., Kirwan, M. L., van der Wal, D., Herman, P. M. J., Dakos, V., Kéfi, S., Scheffer, M., Guntenspergen, G. R. & Bouma, T. J. (2017). Vegetation recovery in tidal marshes reveals critical slowing down under increased inundation. *Nat. Commun.* **8**, 15811, [10.1038/ncomms15811](https://doi.org/10.1038/ncomms15811).
11. Wang, C. & Temmerman, S. (2013). Does biogeomorphic feedback lead to abrupt shifts between alternative landscape states?: An empirical study on intertidal flats and marshes. *J. Geophys. Res. Earth Surf.* **118**, 229–240, [10.1029/2012JF002474](https://doi.org/10.1029/2012JF002474).
12. Himmelstein, J. D. *Mechanisms of Pond Expansion on the Saltmarshes of the Blackwater National Wildlife Refuge, Maryland*. Master's thesis, The College of William and Mary (2018).
13. Bellucci, L., Frignani, M., Cochran, J., Albertazzi, S., Zaggia, L., Cecconi, G. & Hopkins, H. (2007). 210pb and 137cs as chronometers for salt marsh accretion in the Venice Lagoon – links to flooding frequency and climate change. *J. Environ. Radioact.* **97**, 85–102, [10.1016/j.jenvrad.2007.03.005](https://doi.org/10.1016/j.jenvrad.2007.03.005).
14. Roner, M., D'Alpaos, A., Ghinassi, M., Marani, M., Silvestri, S., Franceschinis, E. & Realdon, N. (2016). Spatial variation of salt-marsh organic and inorganic deposition and organic carbon accumulation: Inferences from the Venice lagoon, Italy. *Adv. Water Resour.* **93**, Part B, 276–287, [10.1016/j.advwatres.2015.11.011](https://doi.org/10.1016/j.advwatres.2015.11.011).